Recent developments in the LEMING experiment

A. Antognini, E. Dourassova, K. Kirch, F. Lancellotti, R. Gartner, D. Goeldi,
C. Regenfus, A. Soter, D. Taqqu, R. Waddy, P. Wegmann, S. Werlen
Institute for Particle Physics and Astrophysics, ETH Zurich, 8093 Zurich, Switzerland

M. Bartkowiak, K. Jefimovs, A. Knecht, R. Scheuermann
Paul Scherrer Institute, 5232 Villigen-PSI, Switzerland

F. Wauters
Johannes Gutenberg University of Mainz, 55122 Mainz, Germany

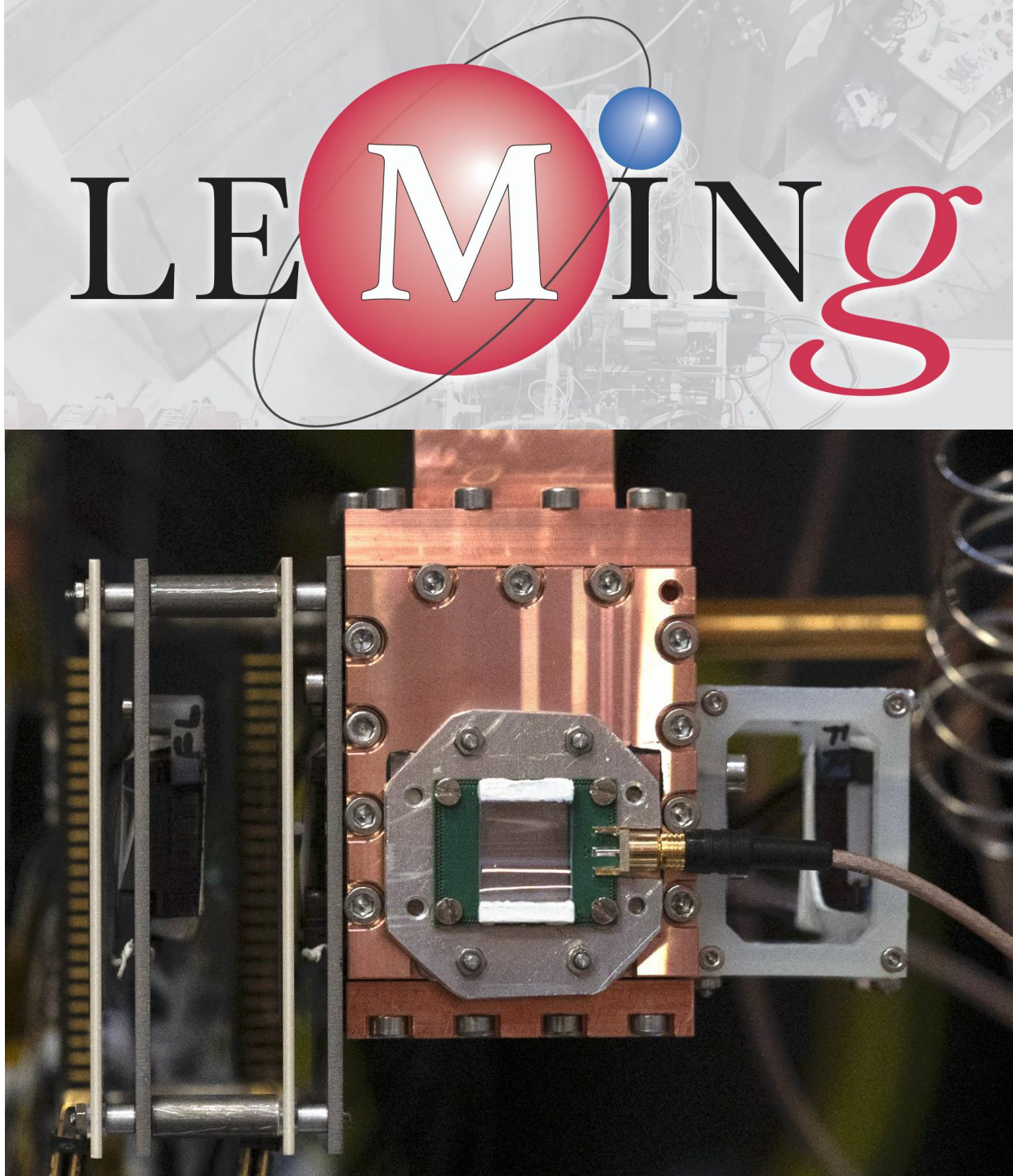

Muonium as a precision probe

Muonium is an interesting system to test fundamental constants and current theories:

- Purely leptonic system dominated by QED effects
- Test of bound-state QED and symmetries (q_μ/q_e)
- Effects on other precision experiments, e.g. muon g-2

Tested through laser spectroscopy of 1S-2S [1], hyperfine structure [2] and Lamb shift [3].

$$E(1s-2s) \simeq \tfrac{3}{4} q_e q_\mu R_\infty \left(1 - \frac{m_e}{m_\mu}\right) + \mathrm{QED} + \ldots$$

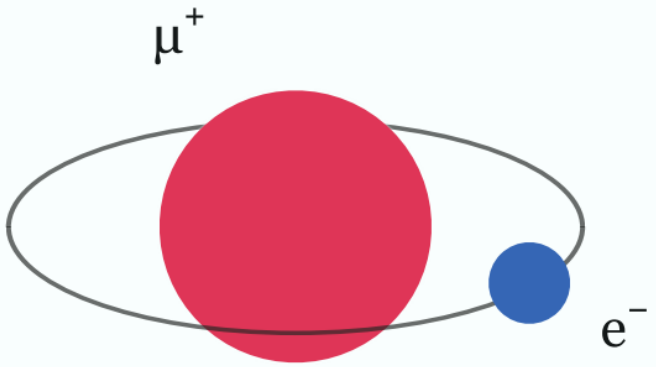

[1] https://doi.org/10.1140/epjd/s10053-025-00960-9
[2] Phys. Lett. B 815, 136154 (2021)
[3] Phys. Rev. Lett. 128(1), 011802 (2022)

Gravity with Muonium

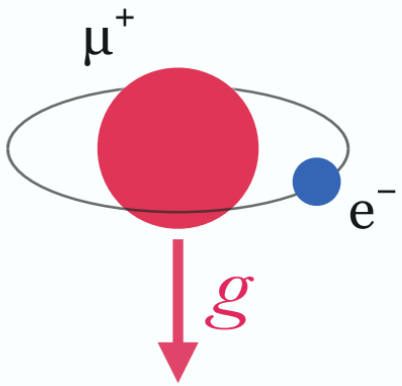

Free fall of Mu

Test of the Weak equivalence principle by measuring the coupling of gravity to:

fundamental parameters of SM, in the absence of masses generated by the strong interaction

second generation (anti)fermions of the SM - only possible probe of this sector

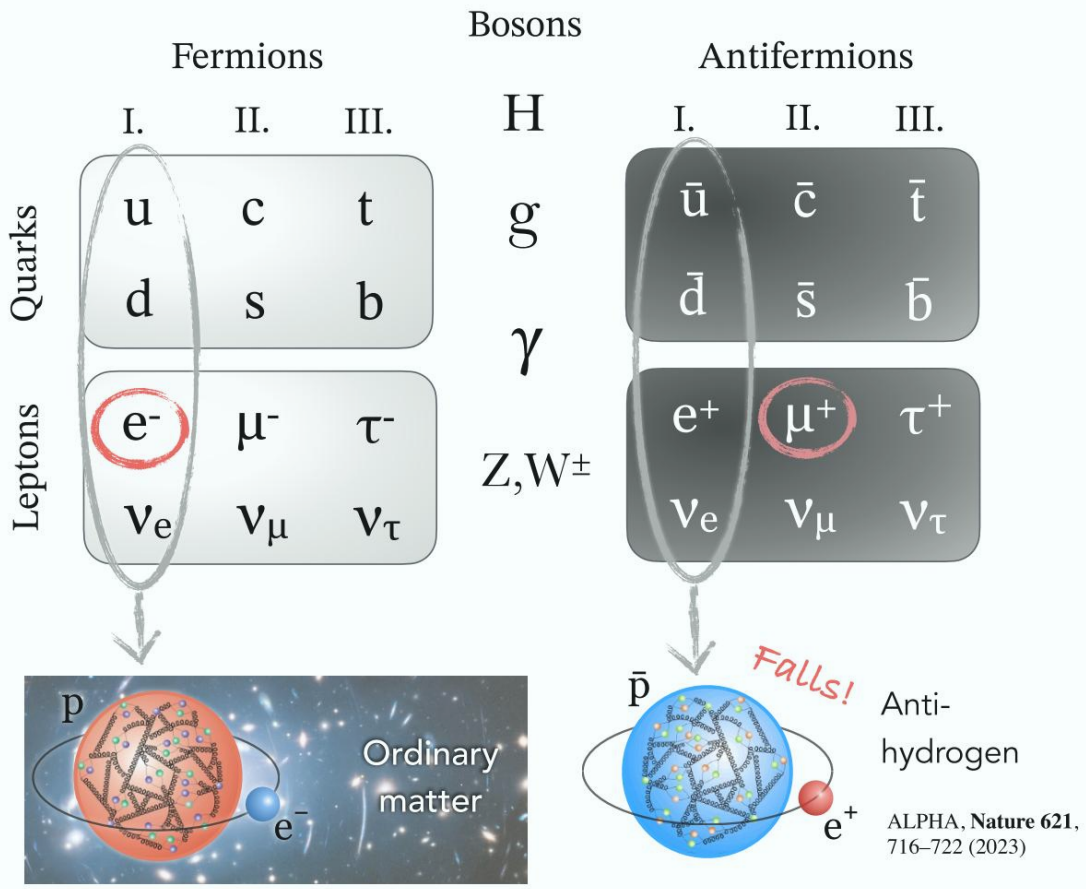

Hadron mass

~1% valence quark

99% strong interaction

Muonium mass

Binding E

μ⁺ mass: 105.6583745(24) MeV/c

e⁻ mass: 0.5109989461(31) MeV/c²

Gravity with Muonium

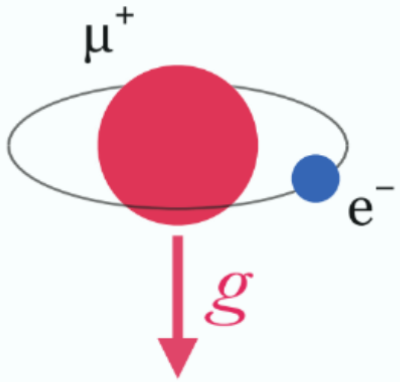

Free fall of Mu

Test of the Weak equivalence principle by measuring the coupling of gravity to:

fundamental parameters of SM, in the absence of masses generated by the strong interaction

second generation (anti)fermions of the SM - only possible probe of this sector

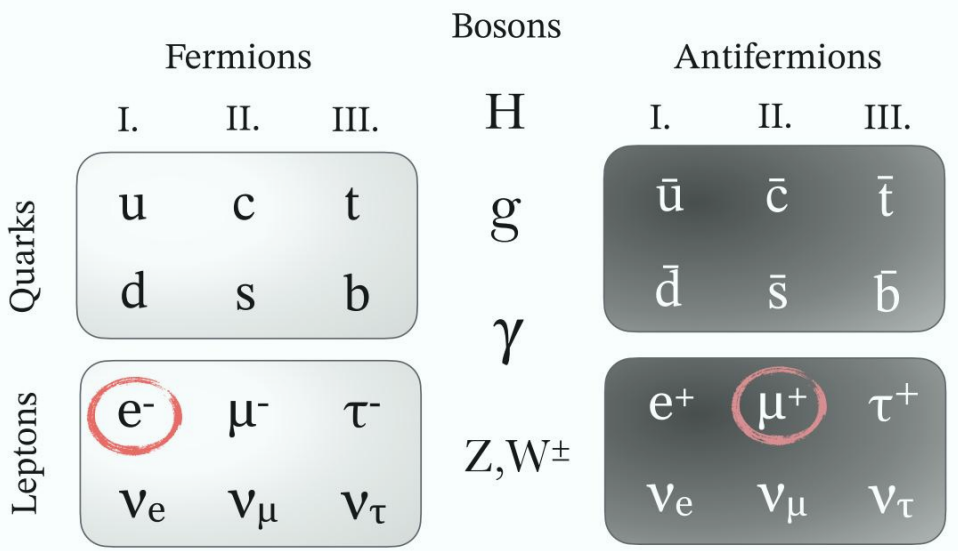

- Possibility to test for flavour-dependent new interactions

Y. Stadnik PRL 131, 011001 (2023)

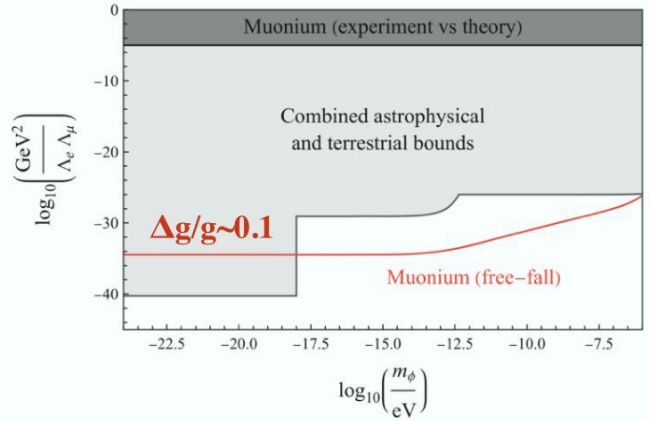

Gravity interferometry with Muonium

Previous sources of Mu were not allowing precise measurement of *g* [1] due to:

- low conversion efficiency (a few percent)
- thermal source
- broad angular distribution

Our newly developed He-II source enables first Mu beam interferometry [2] and muonium spectroscopy [3] with higher precision (~10 MHz -> sub kHz)

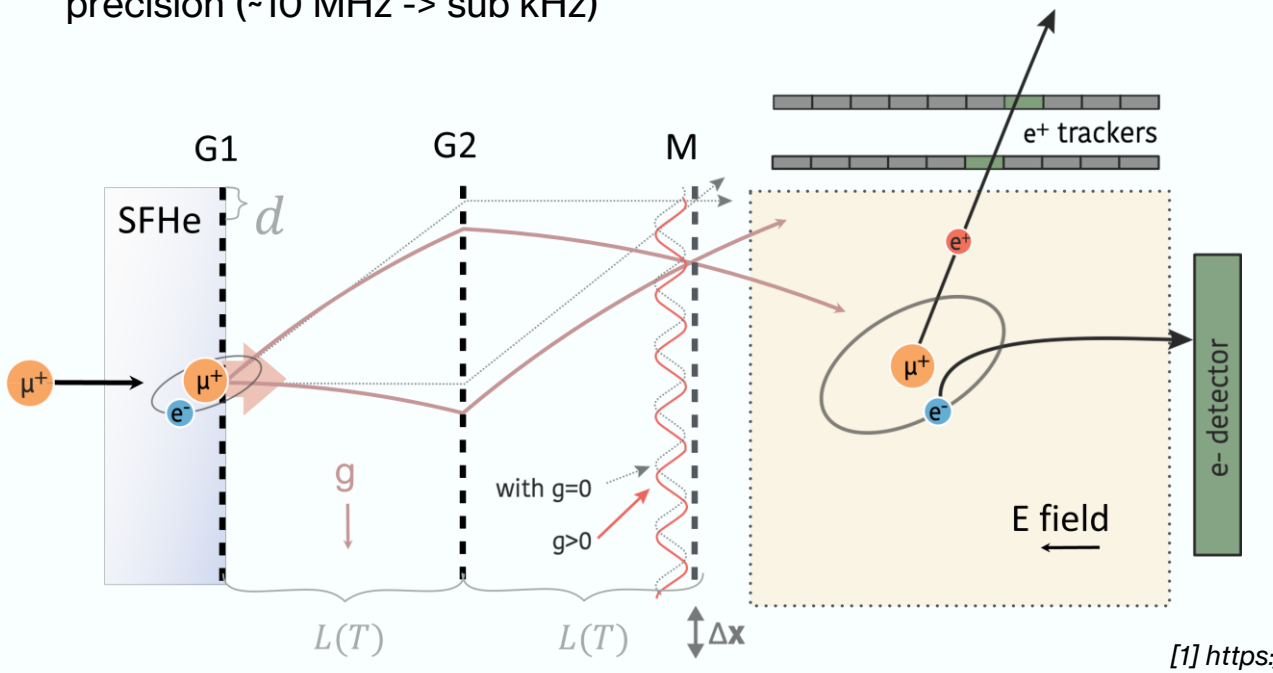

Sensitivity

$$\Delta g \approx \frac{1}{2\pi T^2} \frac{d}{C\sqrt{N_0 \varepsilon \eta^3 e^{-2T/\tau}}}$$

$d = 100$ nm
$T \approx 4$ μs
$L \approx 10$ mm

~ 1% sensitivity

~100 days @ PiE5

[1] https://doi.org/10.1103/PhysRevA.106.052809, https://doi.org/10.1093/ptep/ptaa145
[2] https://doi.org/10.48550/arXiv.2512.19923
[3] https://doi.org/10.1140/epjd/s10053-025-00960-9

Muonium source

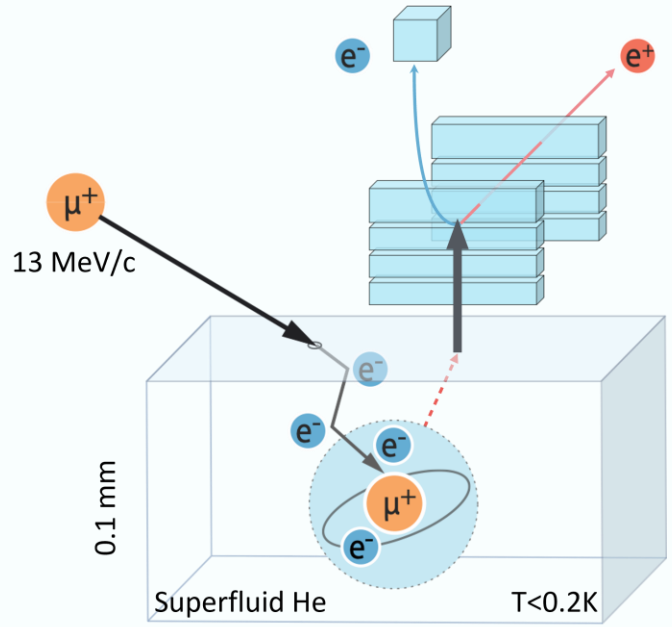

- Low energy muons μ⁺ are stopped in superfluid helium target
- They catch an electron e⁻, creating bound state Muonium (Mu)
- They are transported to the surface and receive a kick from the He-II chemical potential

- **Lowest velocity** Mu source
  $v_x \approx 2175\ m/s$
- **Narrowest** thermal distribution
  $\sigma_{V_x} < 150\ m/s$
- **High yield** similar to the best 300 K sources
  $R(\mu^+ \rightarrow Mu_{vac}) > 8\ \%$
  with $1.5 \times 10^4\ \mu^+/s$
- Suitable for laser spectroscopy

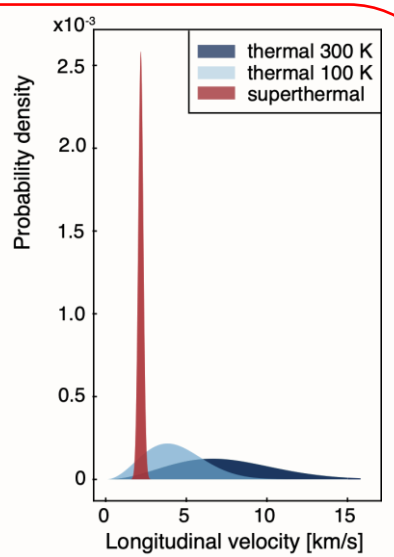

Superthermal

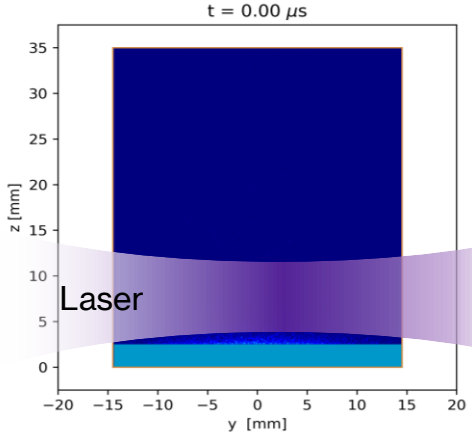

Thermal

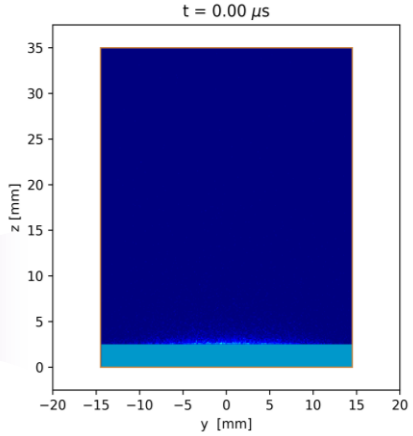

arXiv:2512.19923
(In review - Nature Physics)

Diffusion study

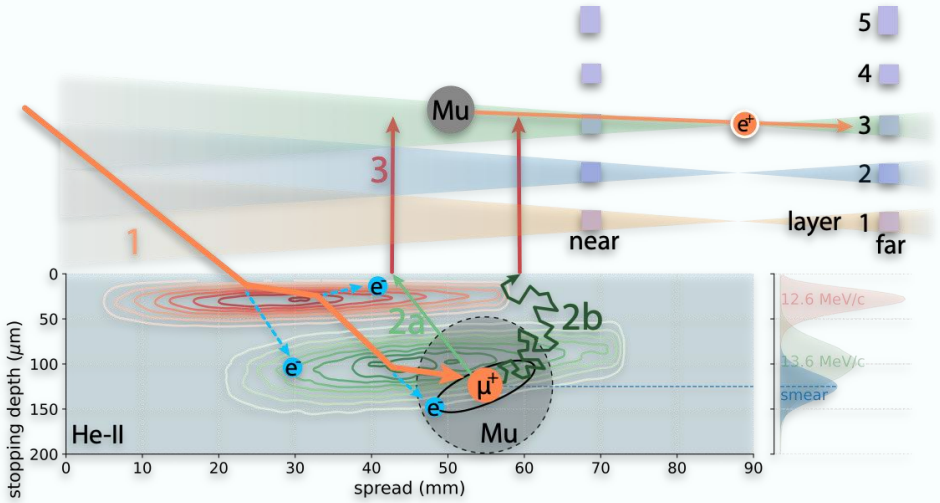

Approach

- Comparison of ballistic and Brownian diffusion
- Bayesian optimization
- 3 free parameters
  - Smearing of stopping distribution σ_smear
  - Diffusion velocity v_dif, or diffusion constant D
  - v_{kick}

Results

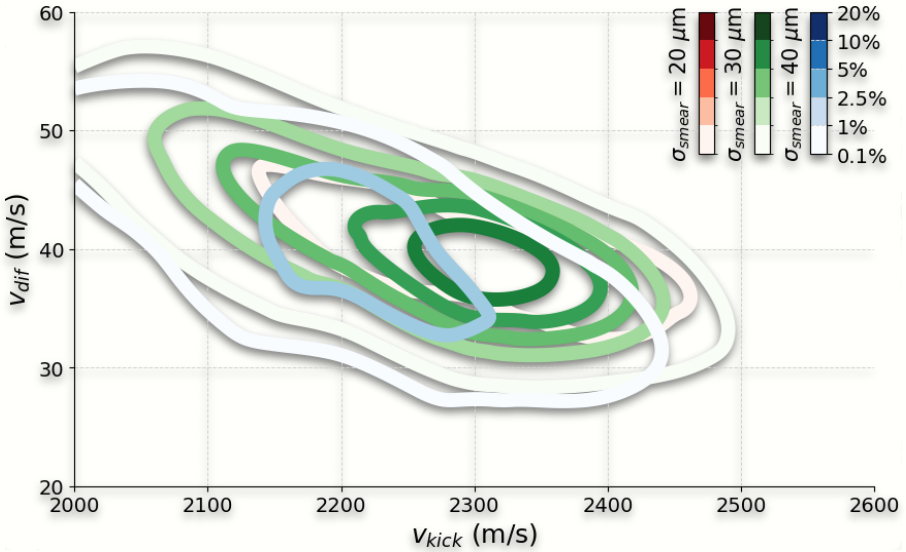

- Rejected Brownian diffusion
- $v_{dif} = 39^{+10}_{-7}$ m/s
- $v_{kick} = 2300^{+120}_{-190}$ m/s
- $\sigma_{smear} = 20^{+10}_{-10}$ μm

Grating integrated source

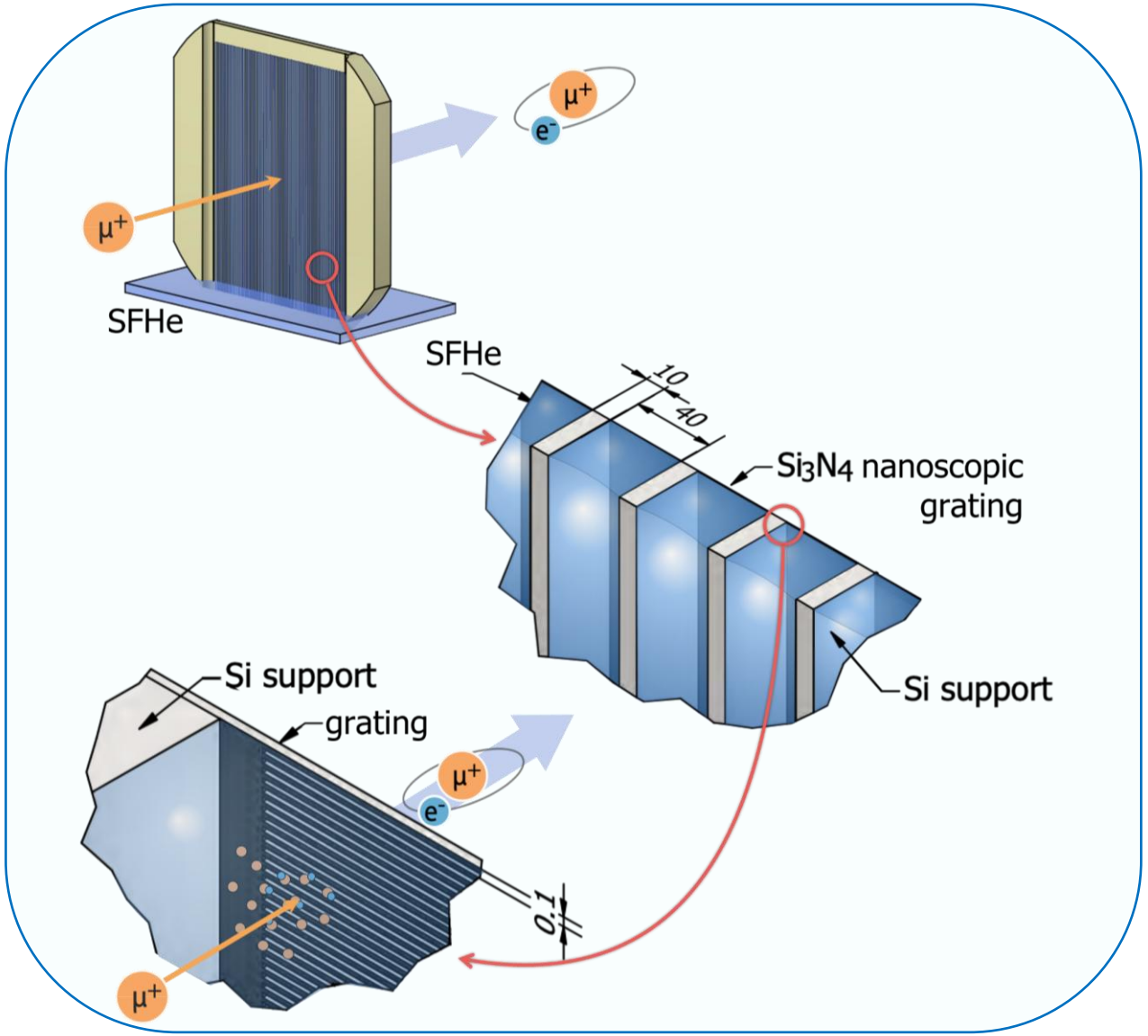

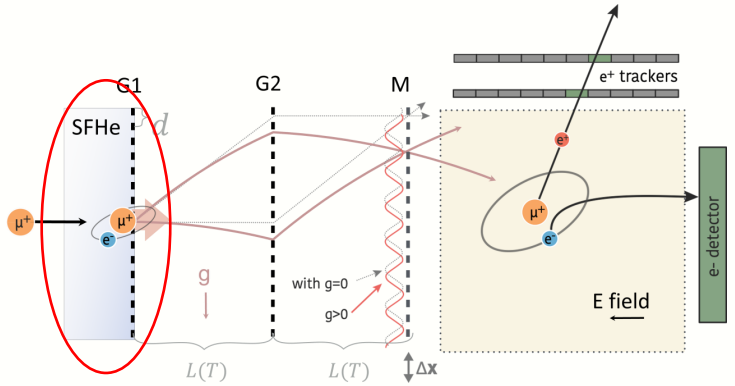

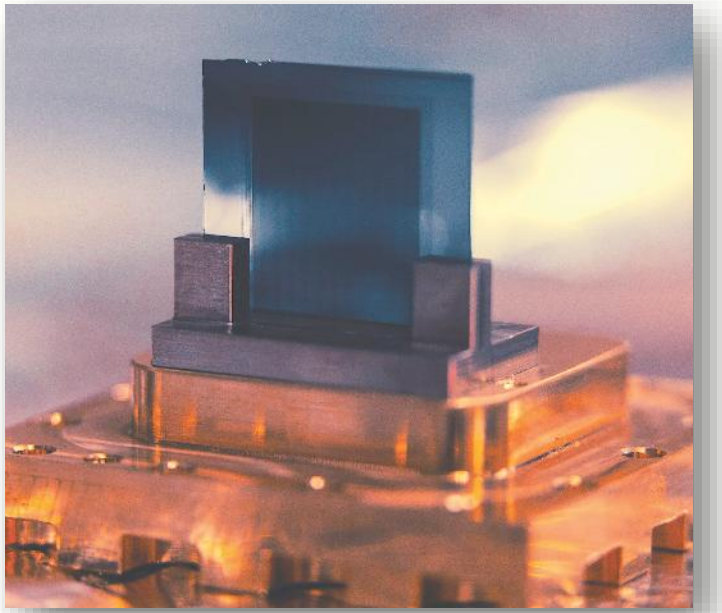

Grating integrated source

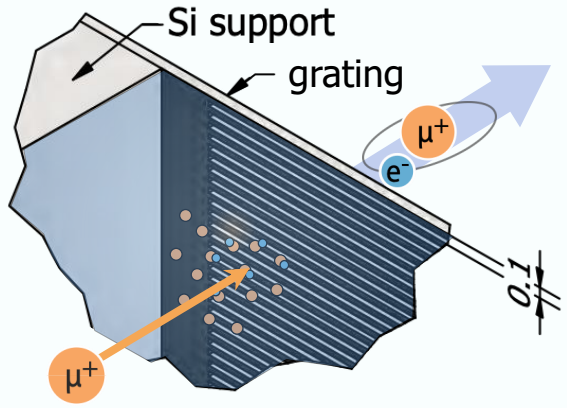

Top view

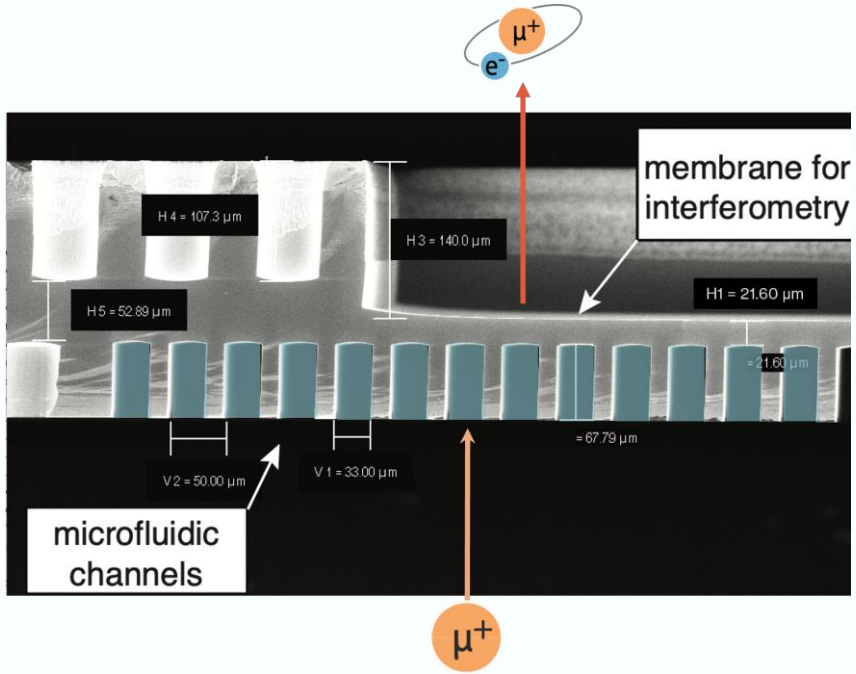

Front view

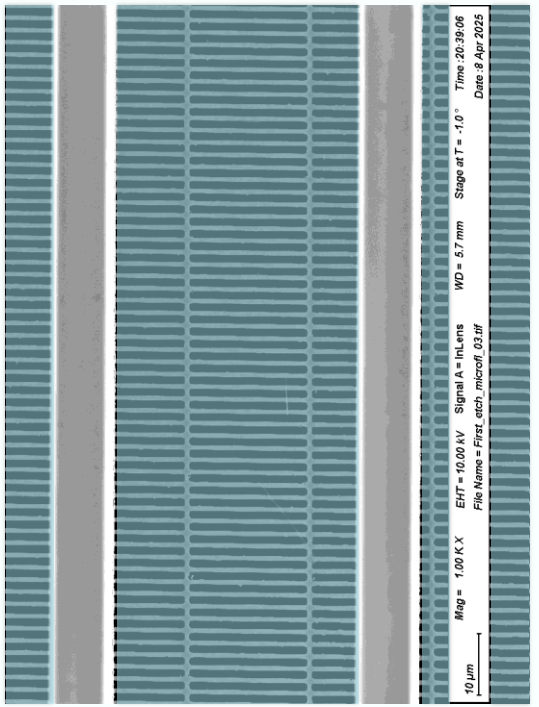

Grating fabrication

Initial monocrystalline silicon substrate

Patterning of He-II microfluidic channels through photolithography and deep reactive-ion etching (DRIE)

Thinning substrate to get thin membrane by means of photo and DRIE

Patterning of alignment holes via electron beam lithography (EBL) and DRIE

Patterning of slits for interferometry by EBL and DRIE

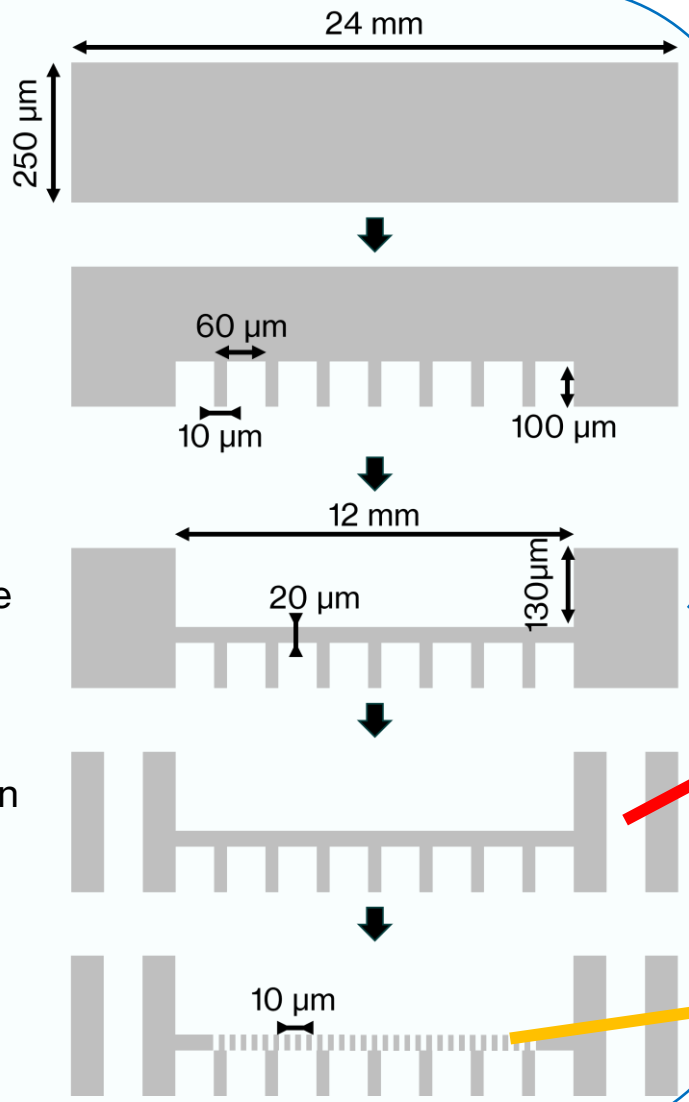

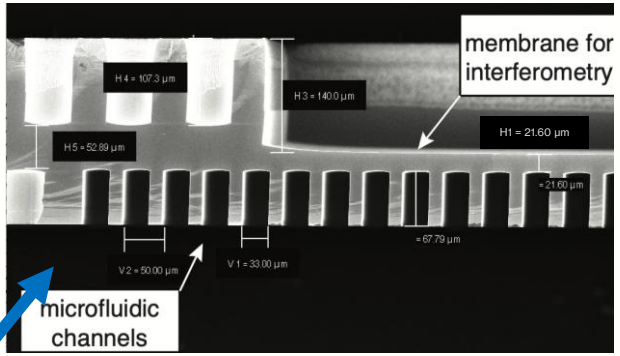

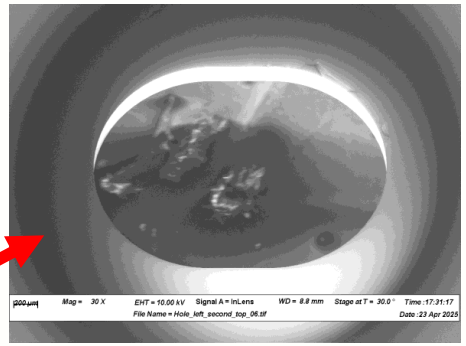

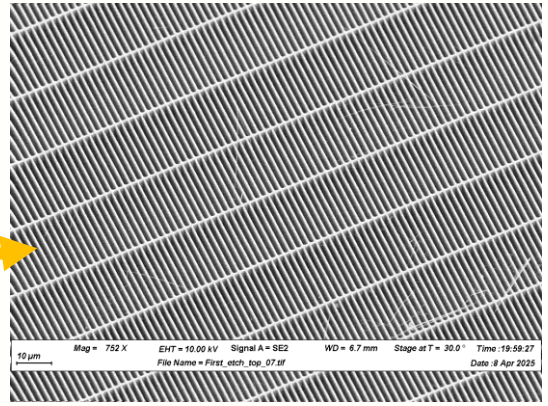

Grating fabrication

Fabricated in PSI
Microlithographic steps with
~10 nm patterning precision
and rotations < 1 µrad

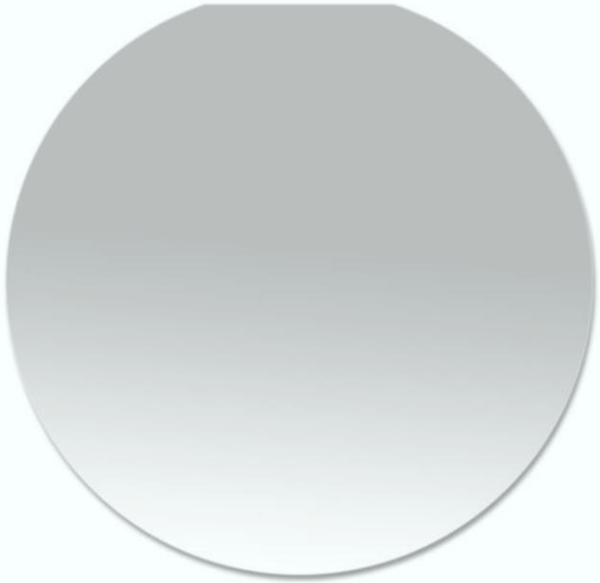

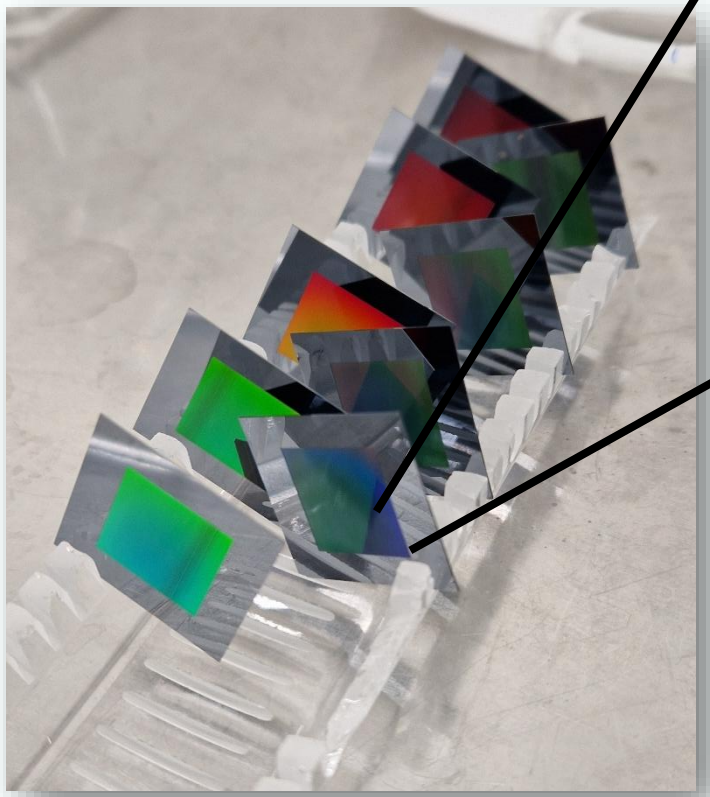

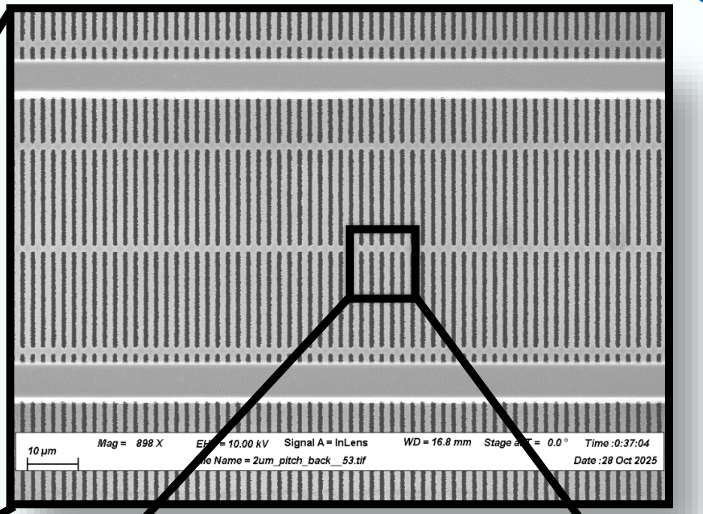

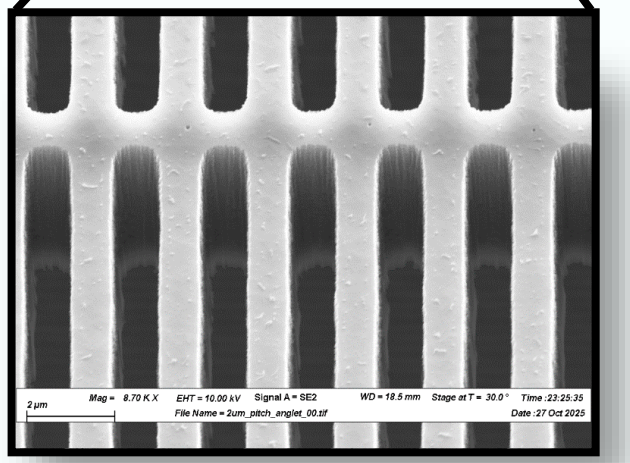

Muonium channels

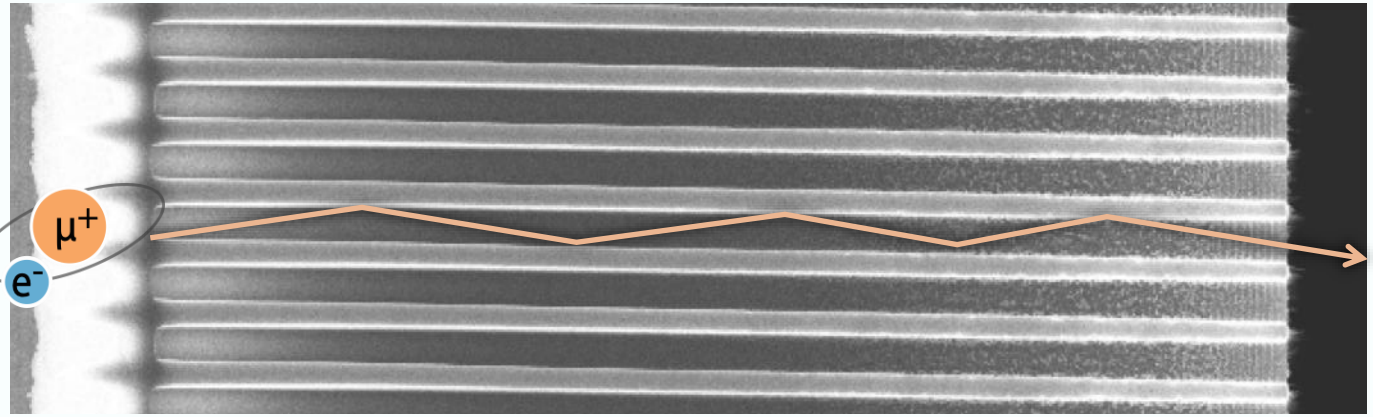

x 0.01

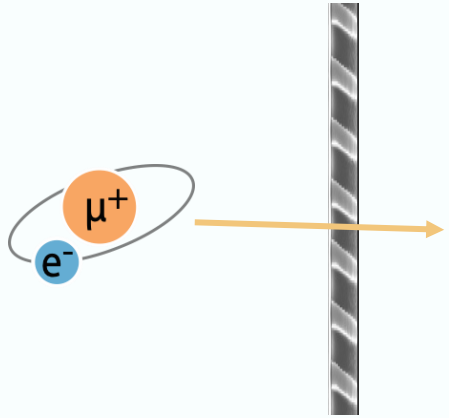

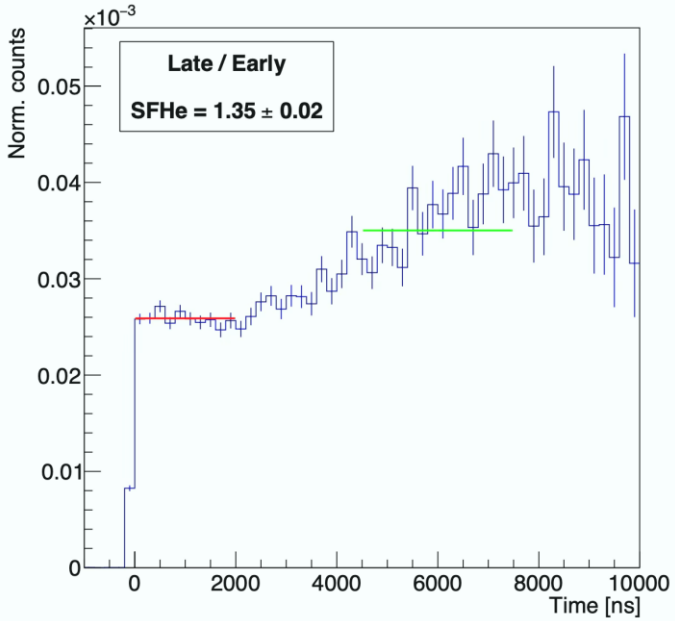

3 times less emission from horizontal bath, but we can optimize with better stopping

Long channels:

- Mu can bounce back from Si or stop
- Increase diffusion time -> lifetime loss

→ Thinner membranes improve muonium emission

Silicon Nitride (Si_3N_4) gratings

Silicon nitride robustness allows fabrication of 250 nm thin membranes

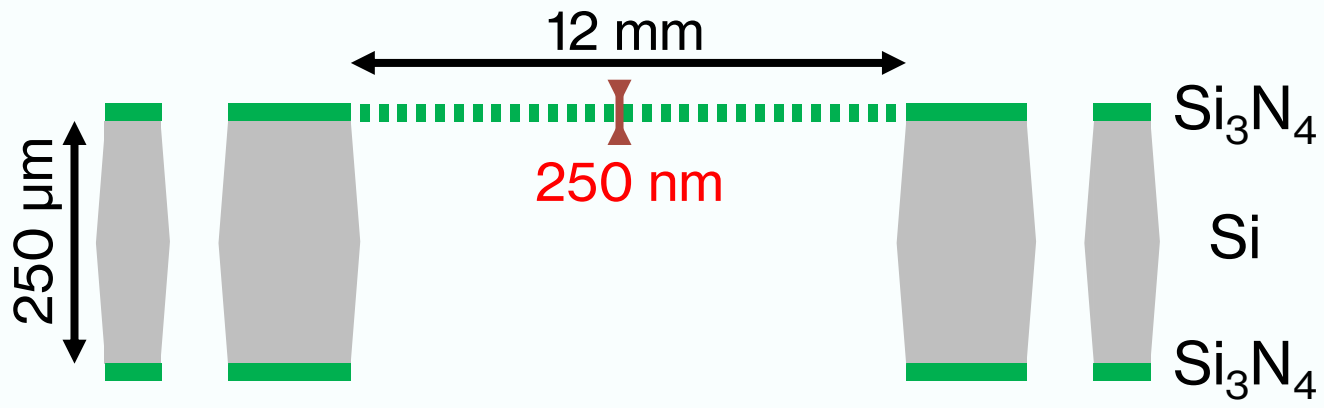

- Silicon nitride with low residual stress (50 - 300 MPa) and high mechanical strength
- Compatible with metalization of membranes for electrical conductivity
- Current development of a more reliable processing of thin membranes

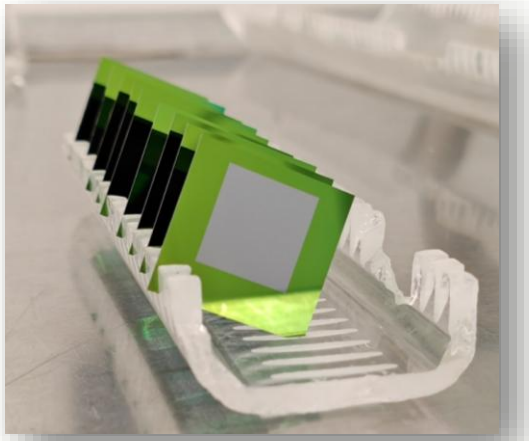

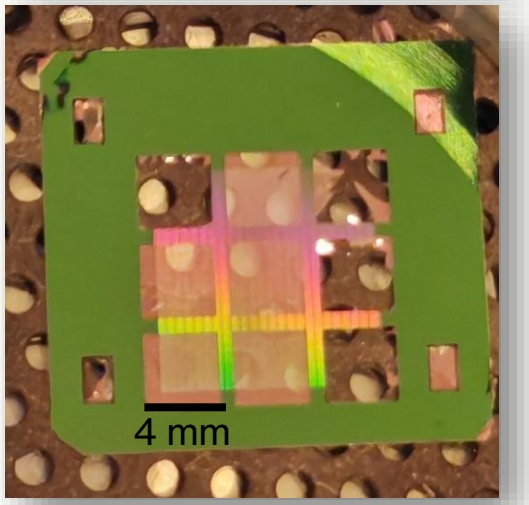

Motion constraints for a gravity sensitive measurement

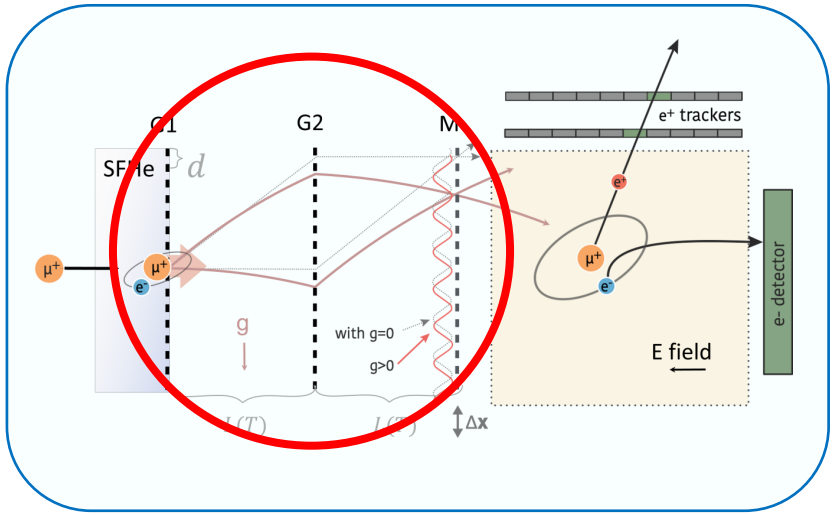

Requirements for 100nm grating:

- Rotation θ_z < 8 µrad
- Tip θ_y < 480 µrad
- Tilt θ_x < 480 µrad
- $L_{12} - L_{23} < 1$ µm

Scanning range $\Delta x = 150$ nm

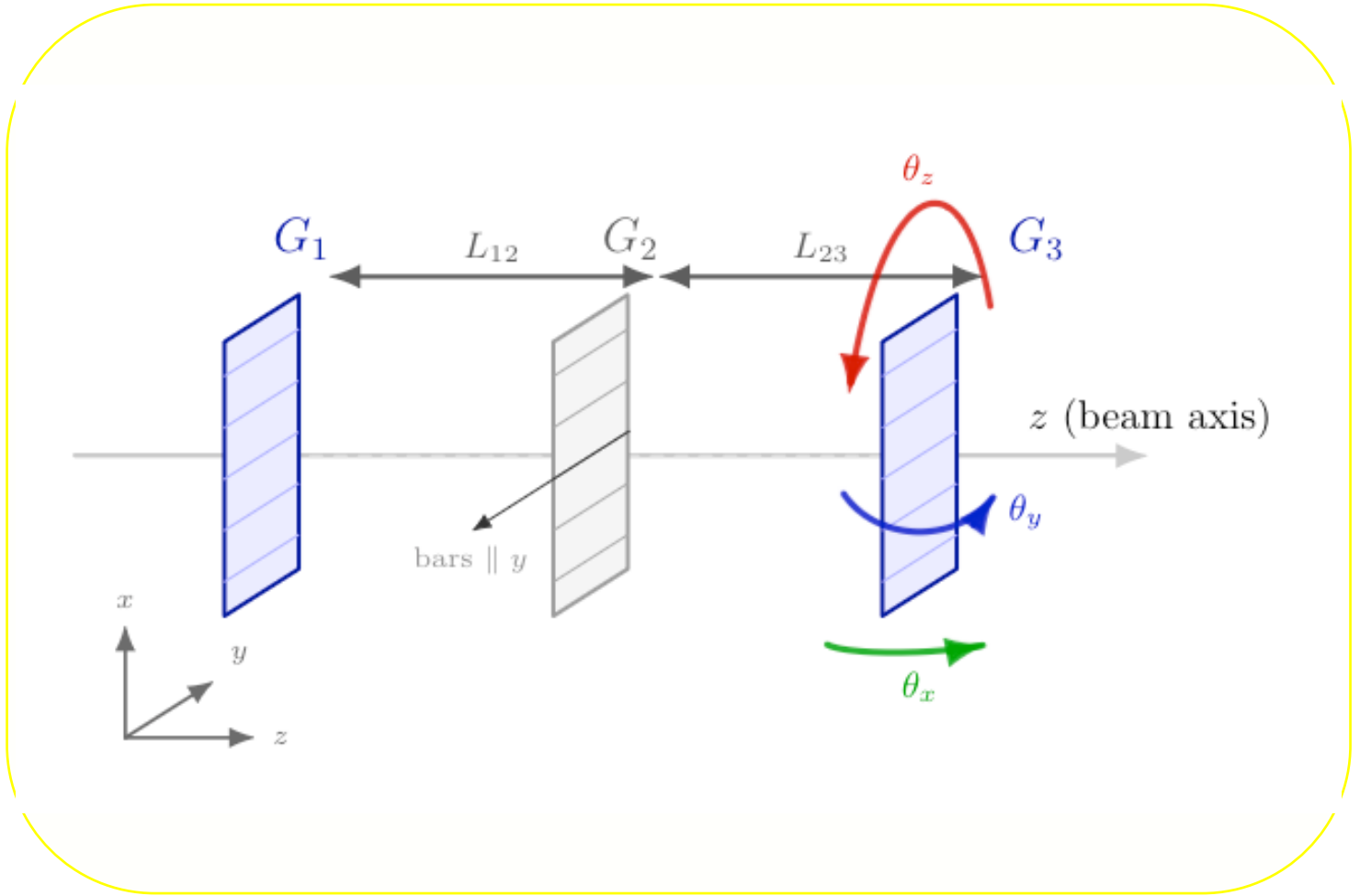

Prototype alignment with precision Si_3N_4 spheres

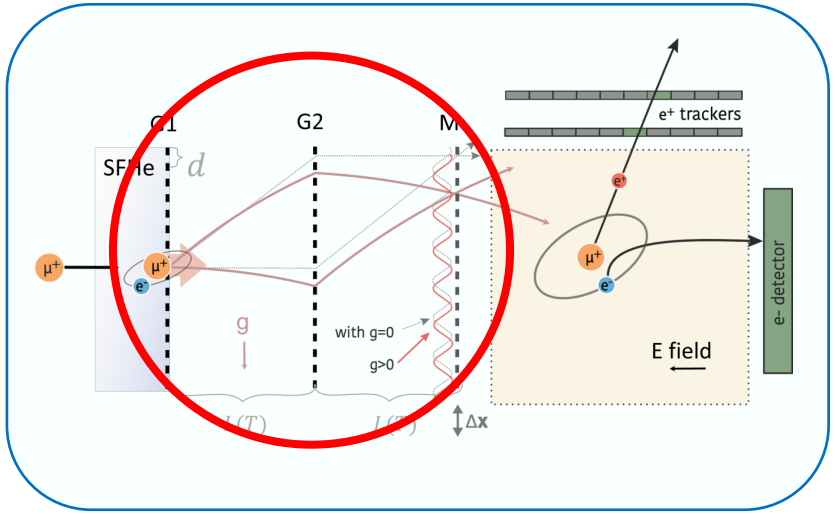

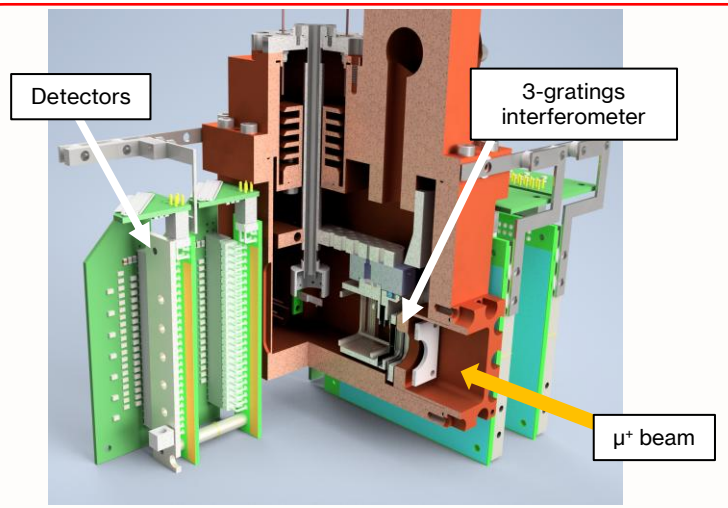

- Self-aligning design for gratings 2 and 3
- Employs Si slots and Si_3N_4 balls

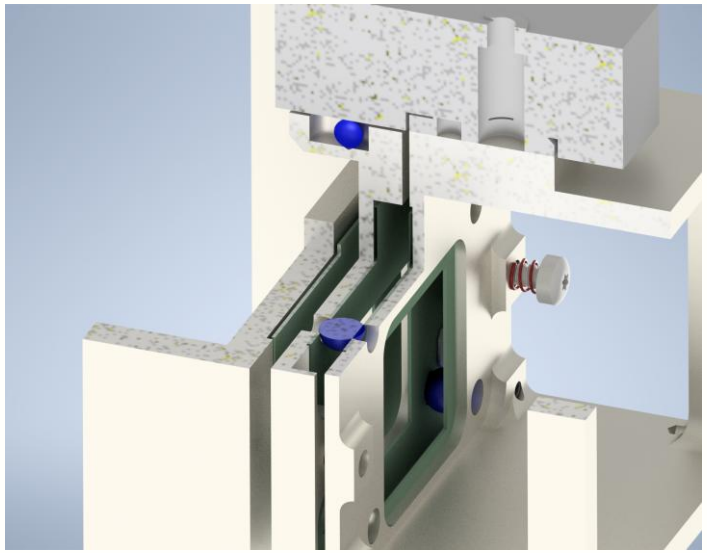

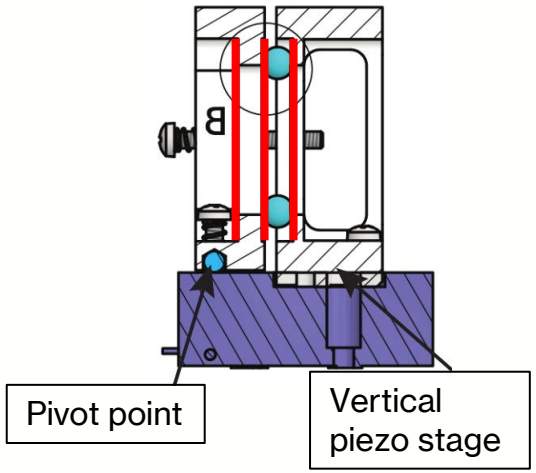

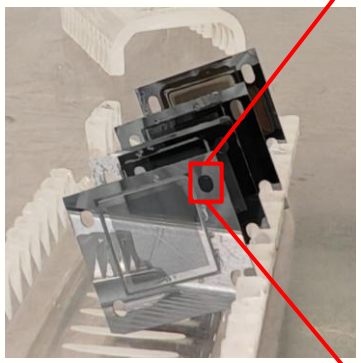

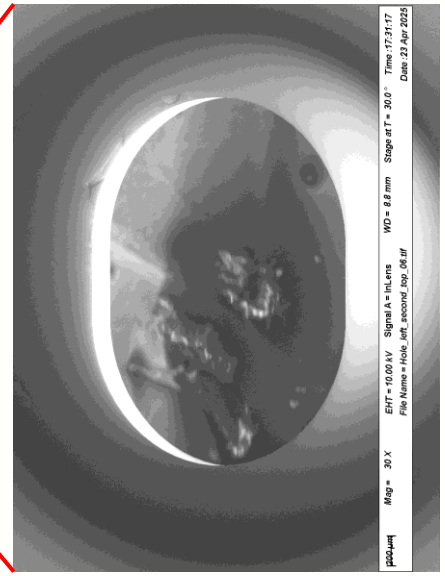

Prototype test - Translation

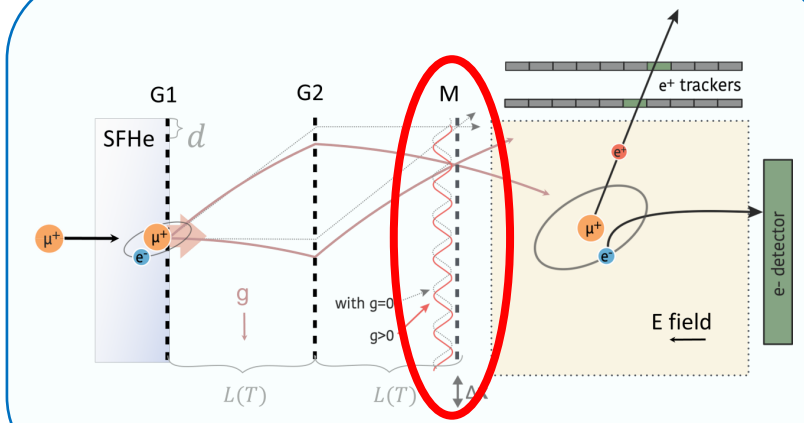

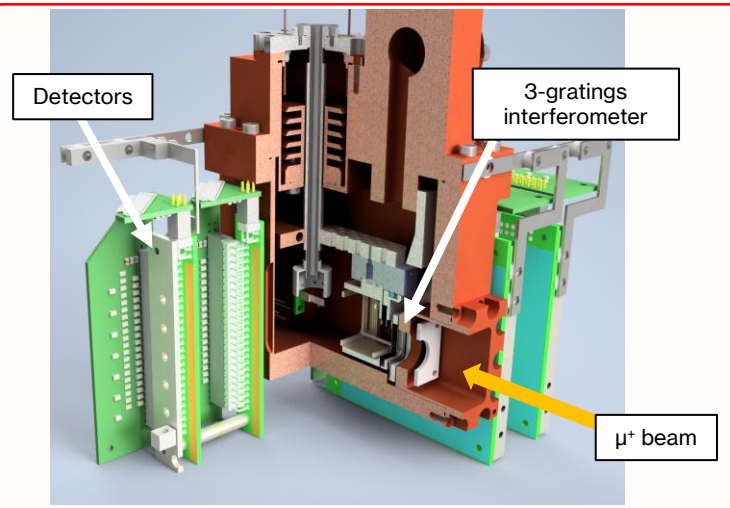

- Self-aligning design for gratings 2 and 3
- Employs Si slots and Si_3N_4 balls

Relative position of the gratings measured with picometer precision via Fabry-Perot cavity

Piezo moving by 17.5 μm along orange axis, with negligible drag of the blue axis

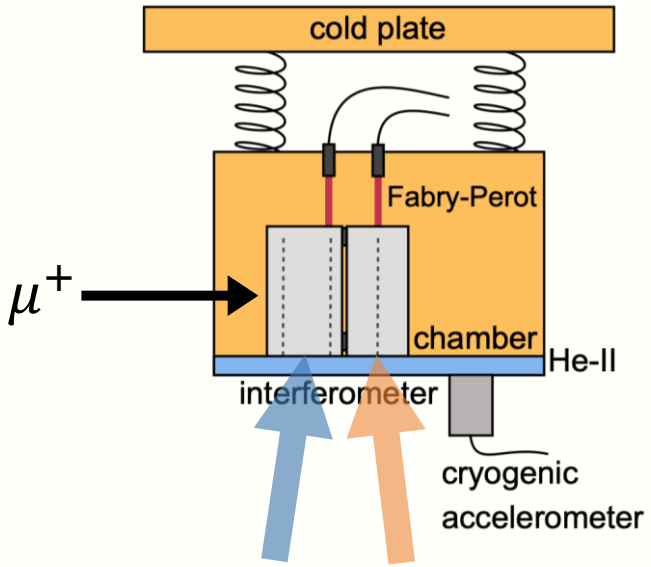

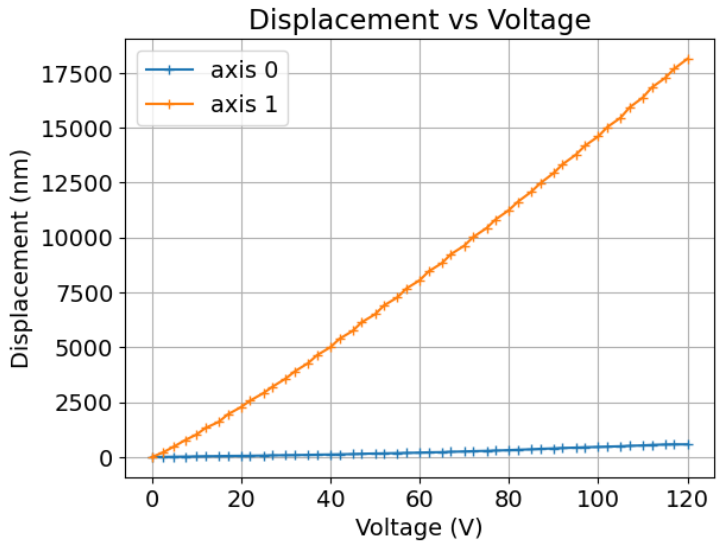

Prototype test - Rotation

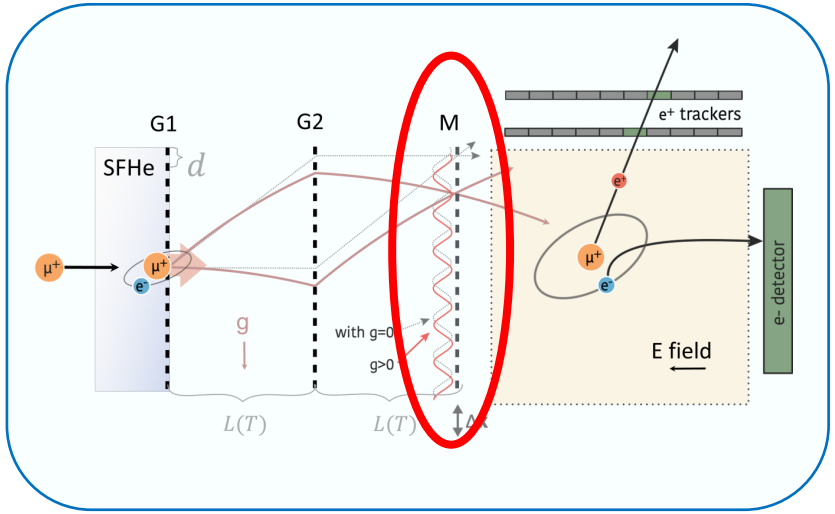

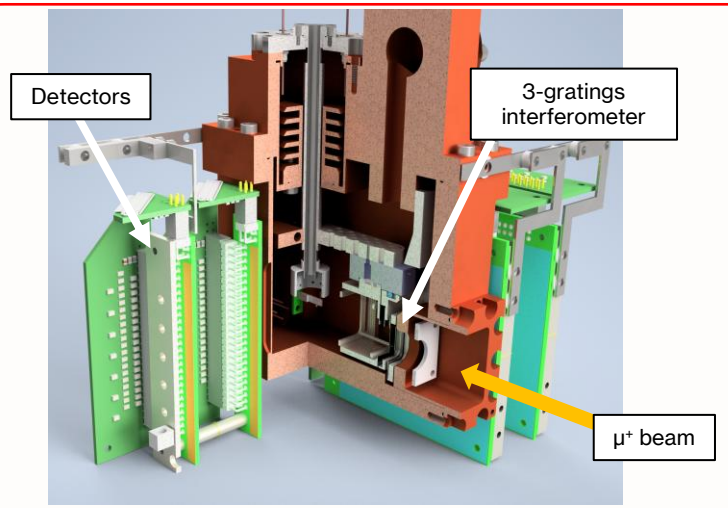

- Self-aligning design for gratings 2 and 3
- Employs Si slots and Si_3N_4 balls

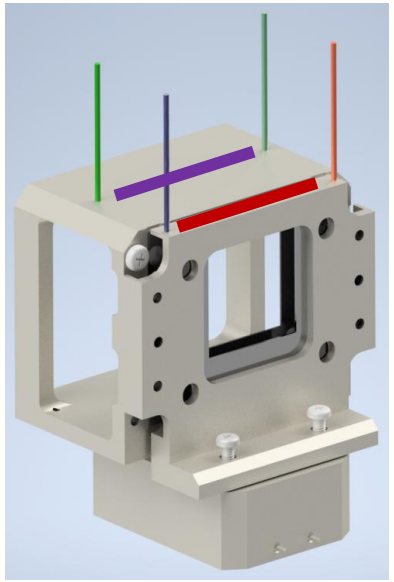

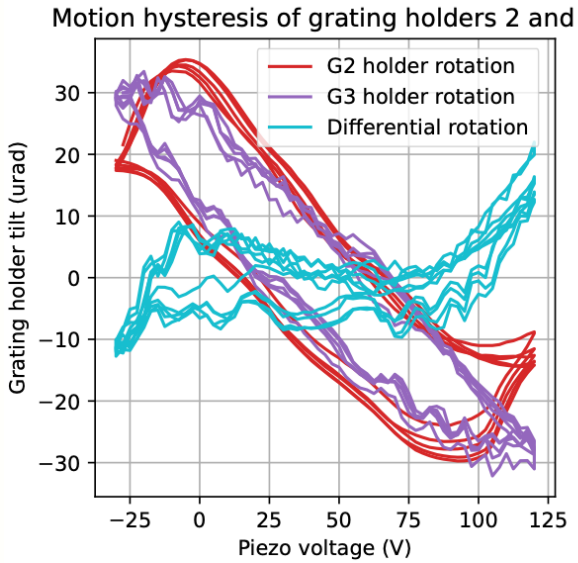

Differential rotation:
30 μrad over 20 μm

Require rotation:
$\theta_z < 160$ μrad over 2 μm

Flexure motion for interferometer

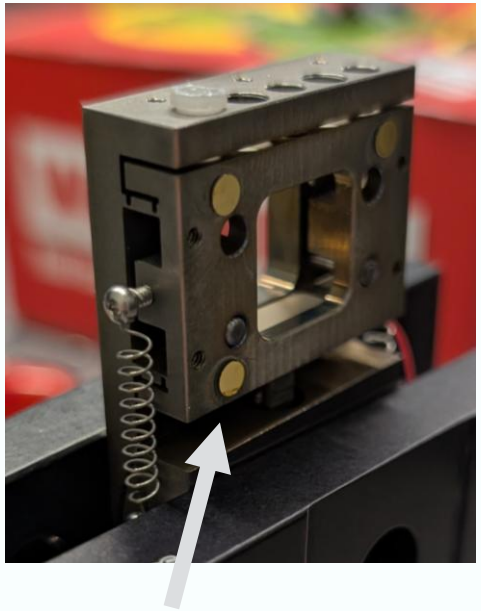

Single parallelogram design

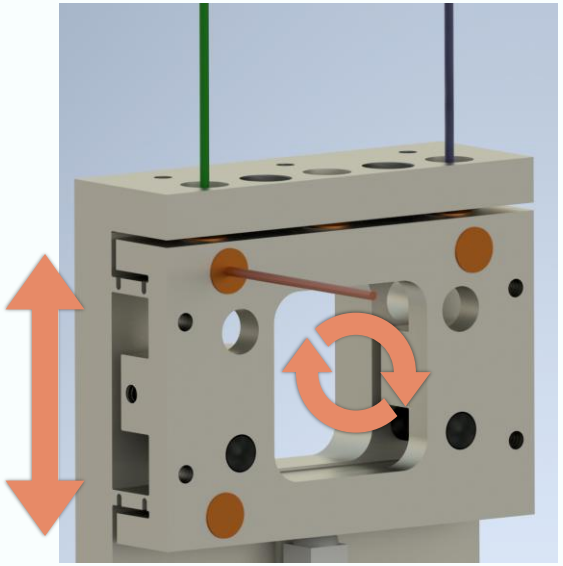

Measured with 3 Fabry-Perot laser cavities

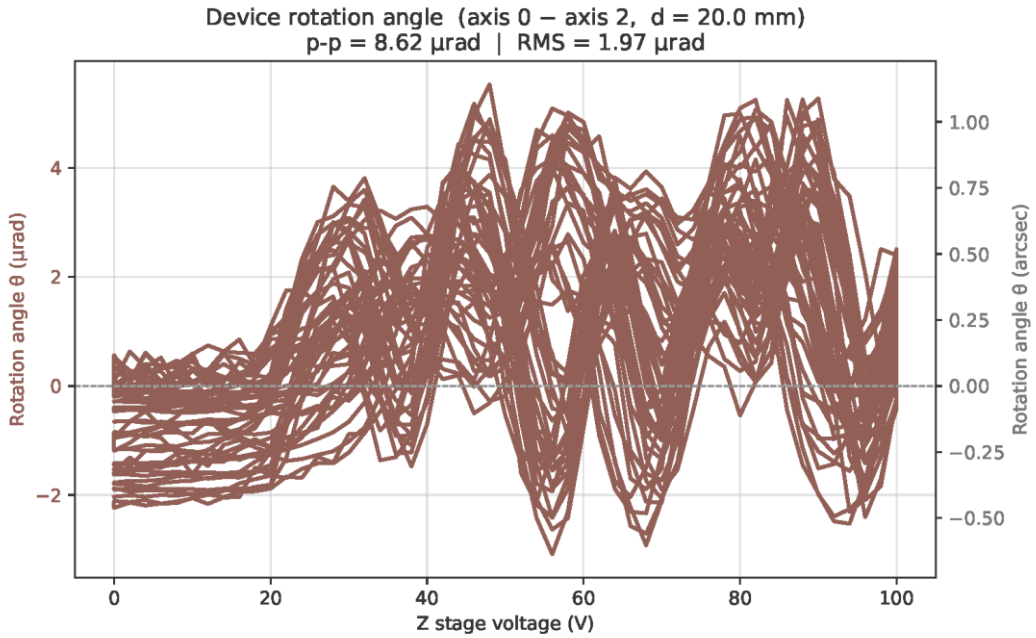

- Rotation constrained to 8.6 µrad over 1.5 µm of motion
- Tip and tilt constrained to 15 µrad and 4.4 µrad respectively

Accuracy and precision met for an interferometer sensitive to gravity

Monolithic design

Flexure design

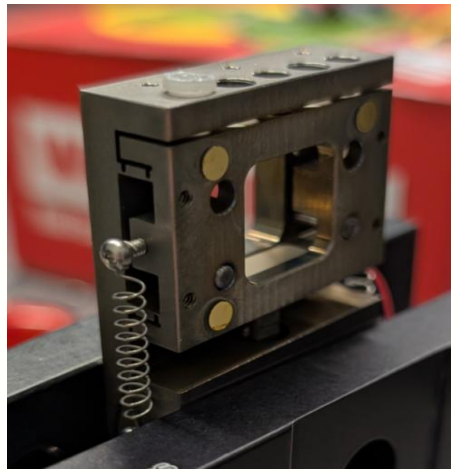

Monolithic design

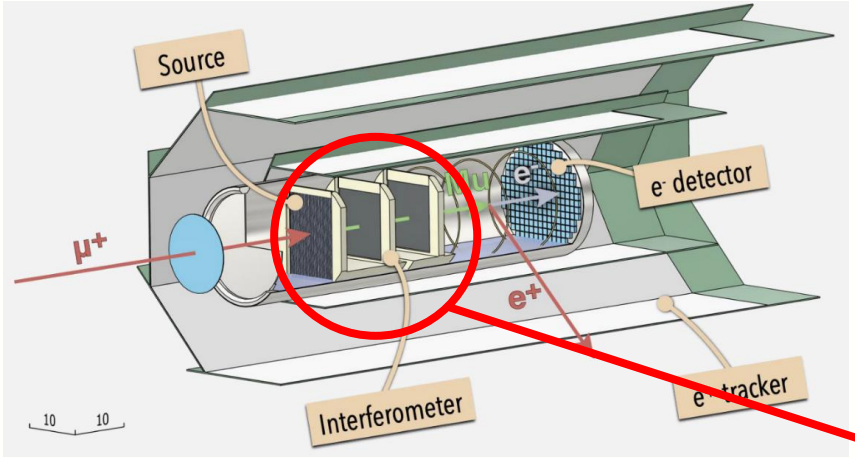

Monolithic design allows for precise alignment of the 3 gratings system

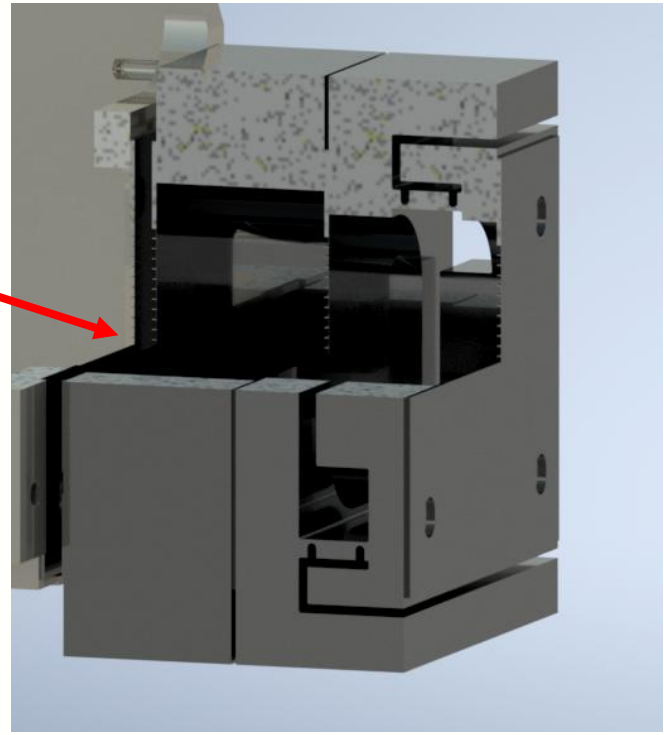

Plans for first interferometry

Coherent source

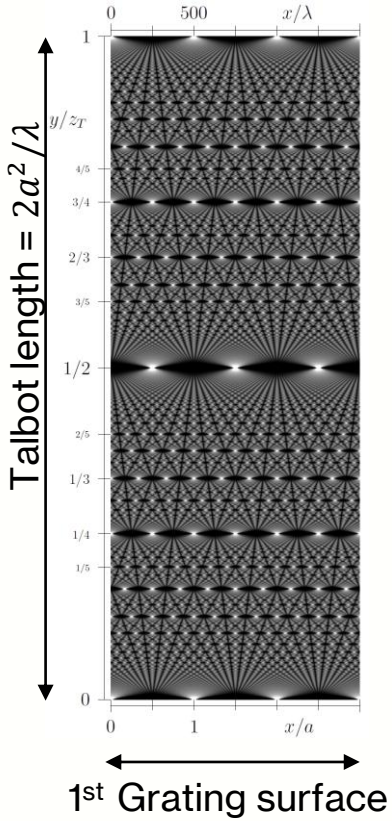

Incoherent source

Single slit source

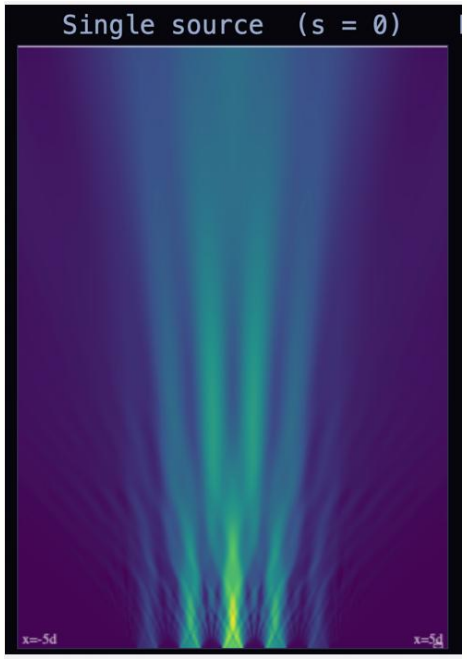

Periodic source

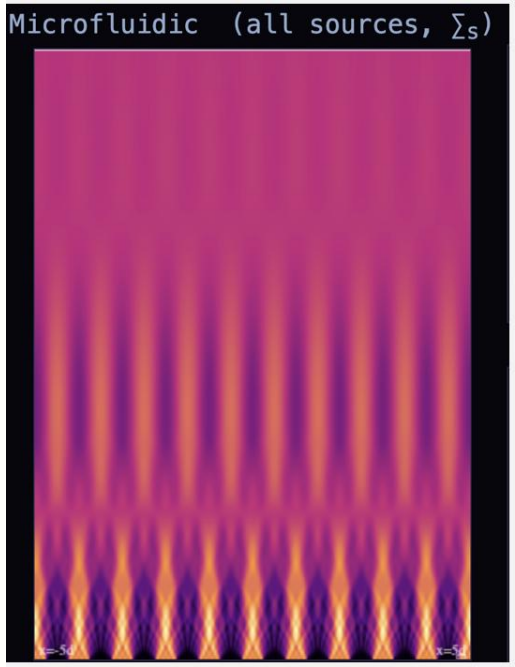

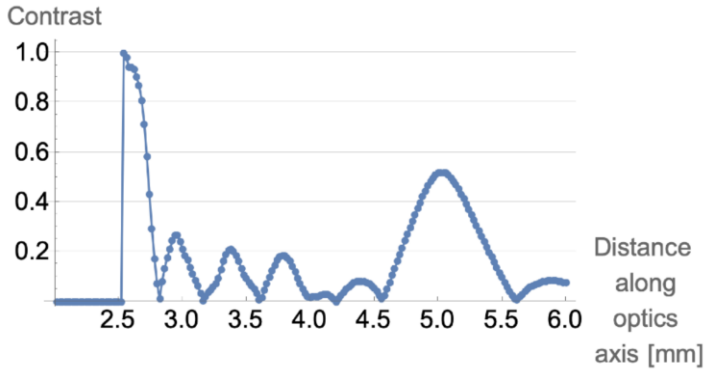

- With slit period of a=2 μm, the Talbot-length of Mu is ~ 5 mm
- Setup is optimized for the 1/2 Talbot length (2.5 mm), with an expected contrast of 0.5

LED test - Static

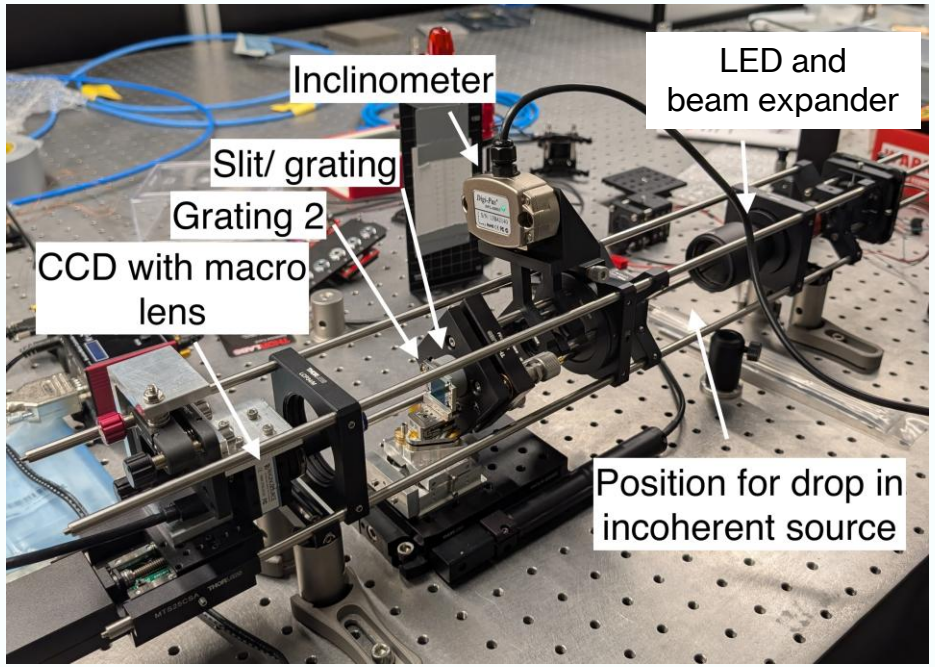

Laser shinning through a single slit and then a grating

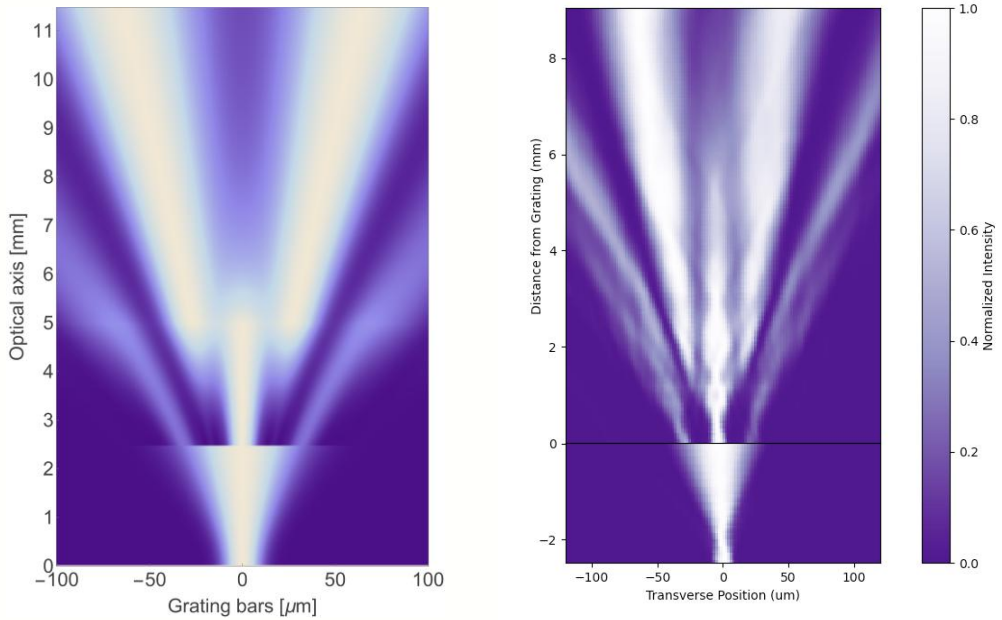

GSM simulation Experiment

Gaussian-Schell model with Mutual intensity function:

$$I_{\mathrm{mf}}(x,z) = I_0 \sqrt{\frac{\pi}{\Delta_v}} \sum_{m,n} a_m a_n \sqrt{\frac{\pi}{A}}\, e^{\frac{2\pi i}{d}(m-n)\bar{x}_{mn}\frac{\pi^2}{A\Delta_v}} e^{-\frac{\pi^2(m-n)^2(\lambda z)^2}{Ad^2}} \sum_{s=-\infty}^{\infty} e^{-\frac{(\bar{x}_{mn}-sd)^2}{2\sigma_I^2}\frac{\pi^2}{A\Delta_v}} e^{-\frac{2\pi i}{d}(m-n)sd\frac{\pi^2}{A\Delta_v}}$$

https://doi.org/10.1103/PhysRevA.78.013601

LED test – Two gratings

Interferometry pattern from two grating
Talbot-Lau interferometer

Check Siegfried's poster

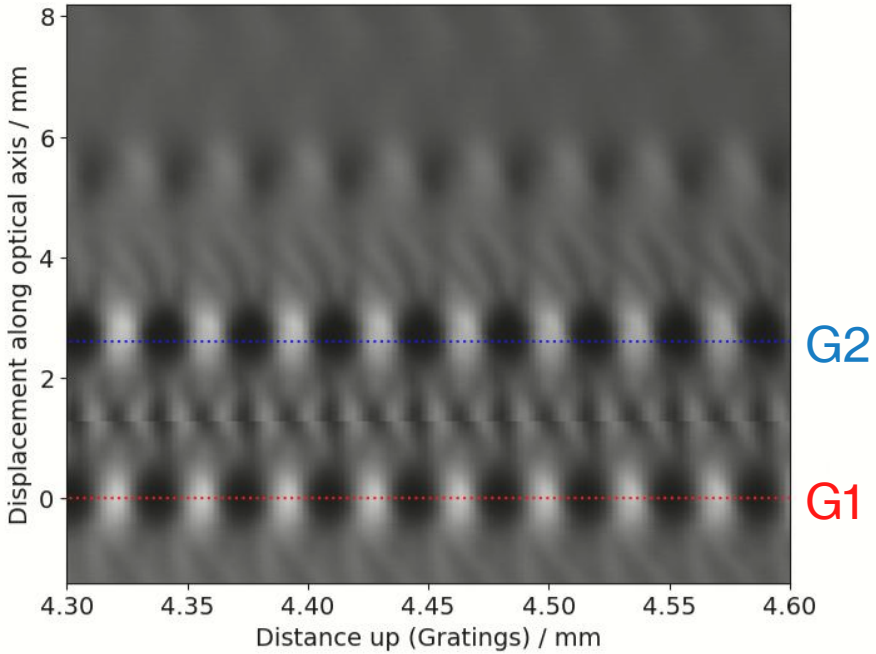

Experiment

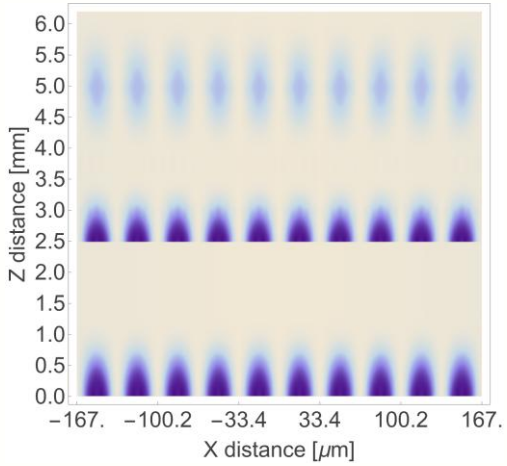

Simulation

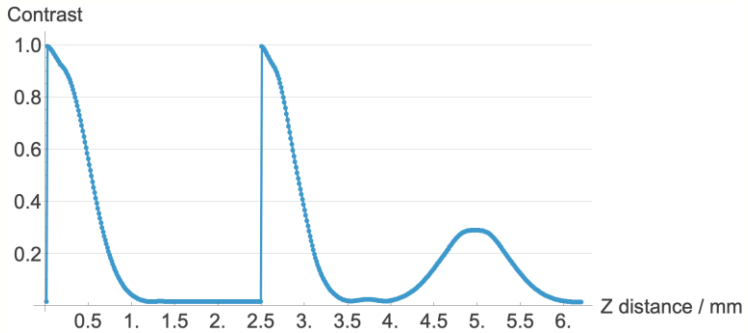

Simulation

Mean contrast of 0.3 (theoretical limit)
at one Talbot length

Outlook

Interferometer monolithic design

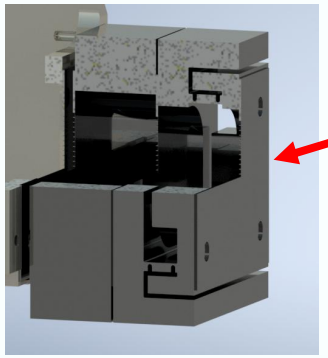

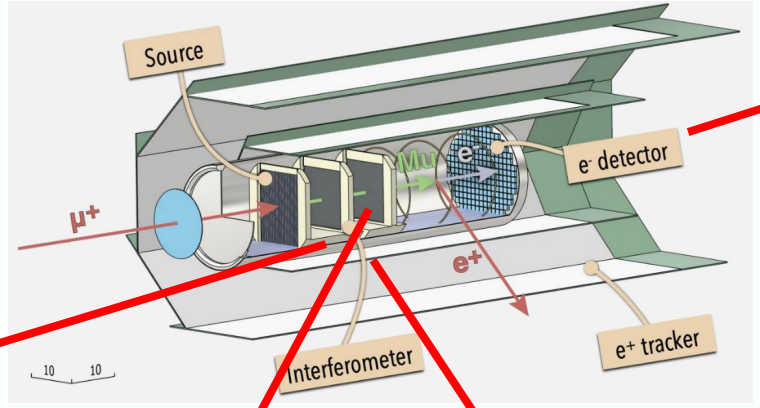

Detectors (Mu, X-ray)

Perovskites CsPbBr3

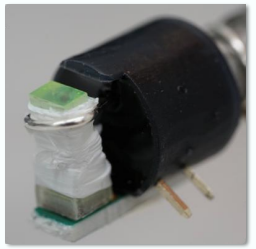

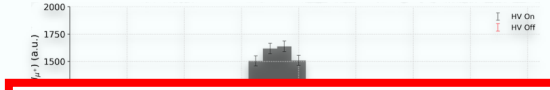

Check Siegfried's poster

Nanowire

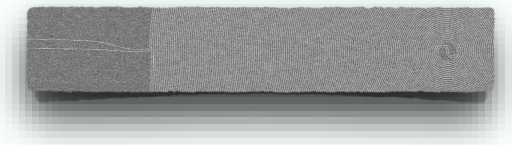

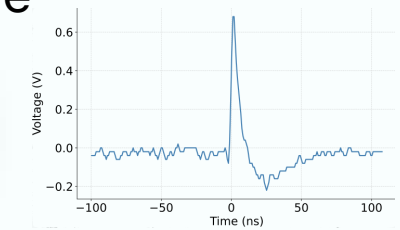

Si_3N_4 gratings

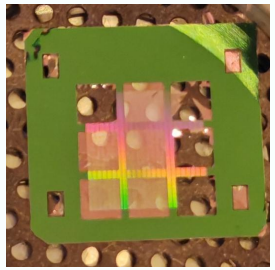

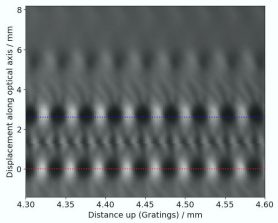

$$E(1s-2s) \simeq \tfrac{3}{4} q_e q_\mu R_\infty \left(1 - \frac{m_e}{m_\mu}\right) + \text{QED} + \ldots$$

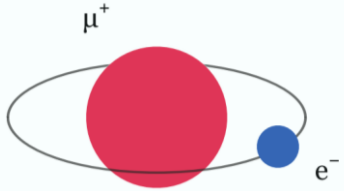

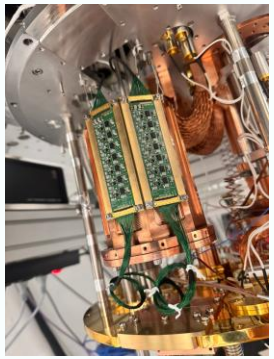

Prospects:

- Perform first gravity measurement with Muonium
- Spectroscopy of 1S-2S transition with lower uncertainty:
  ~10 MHz -> sub kHz

Thank you for your attention!

LEMING

LEptons in Muonium INteracting with Gravity

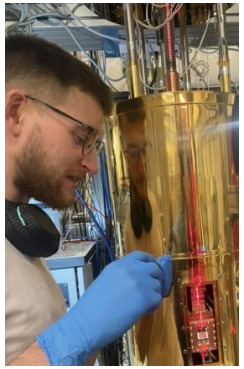

SNSF Starting Grant

Backup

Muonium – probing SM

Not possible with conventional Mu sources

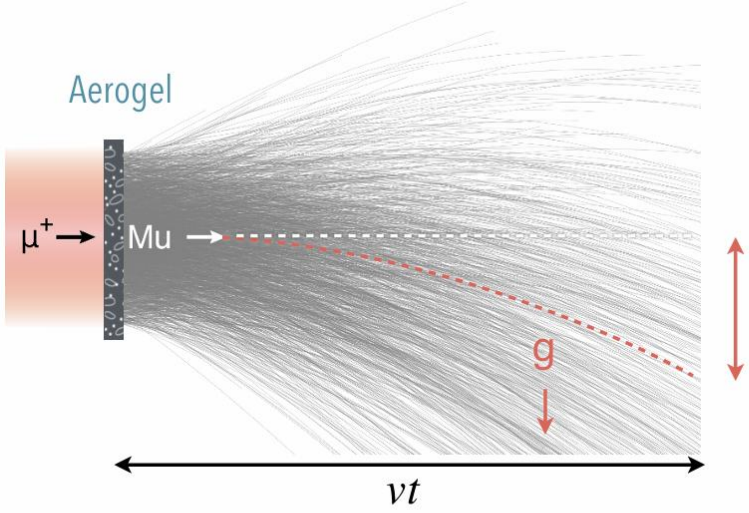

Mu lifetime of 2.2 μs

$$\Delta x = \frac{1}{2} g t^2 < 1 \text{ nm}$$

Why it might be possible with LEMING

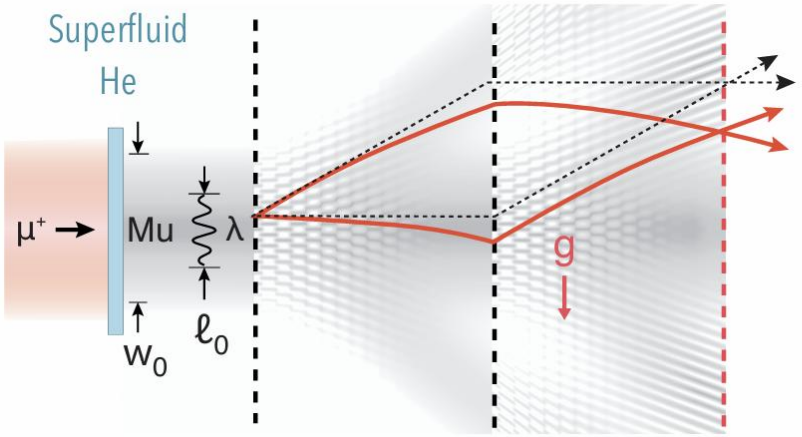

We developed a novel Mu beam amenable to interferometry

Atomic electron detector - Perovskites

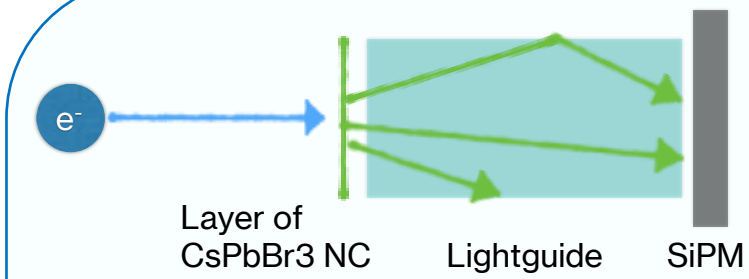

Issues

- Unknown source of background, investigations ongoing
- Afterglow? Failure of SiPM?
- Poor Detection Efficiency
- Poor Collection Efficiencies?

Perovskites
CsPbBr3

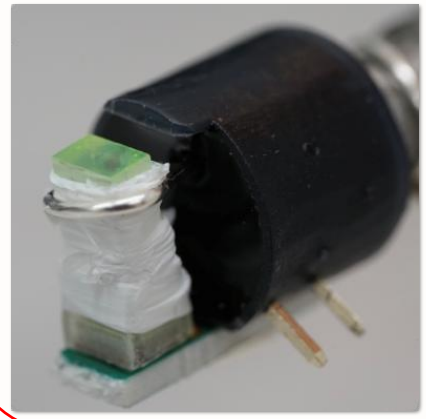

Drift time

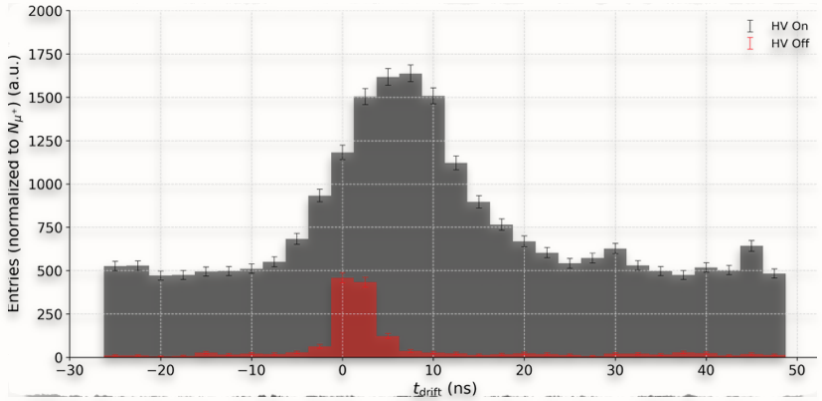

Plastic Scintillator
EJ-204

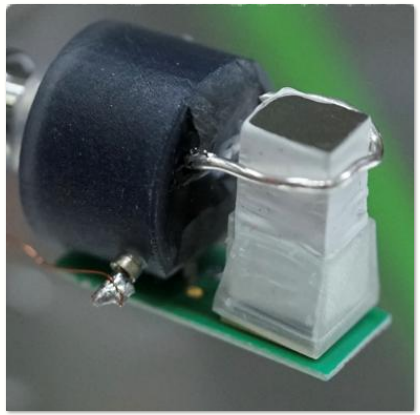

Drift time

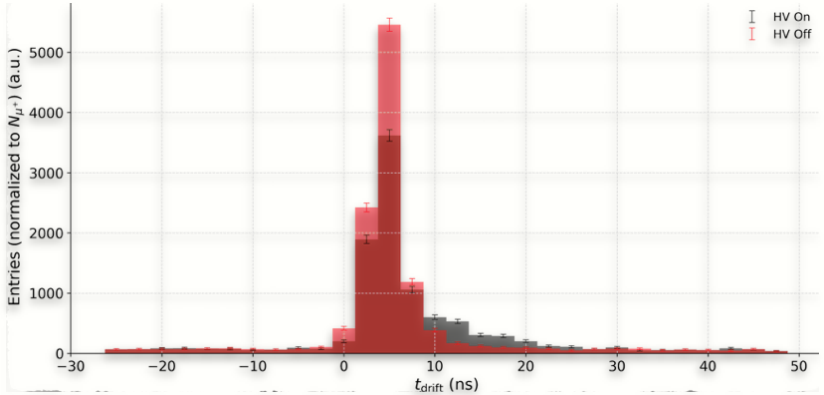

Atomic electron detector - Nanowire

Working Principle

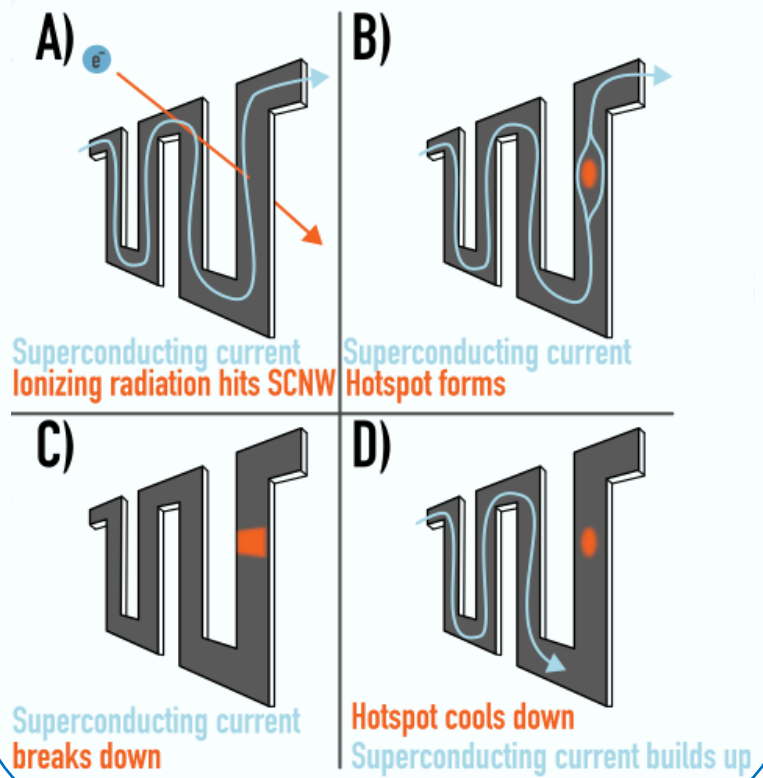

Successful operation

- Detected electrons down to 1 Kev
- Efficiency still needs to be determined

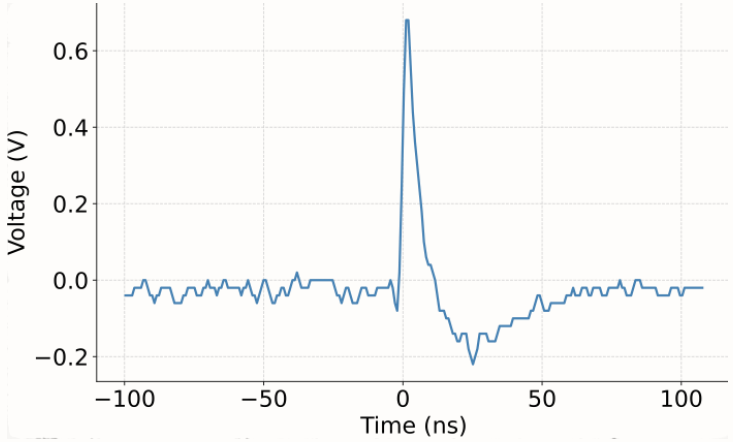

New custom samples SNSPD

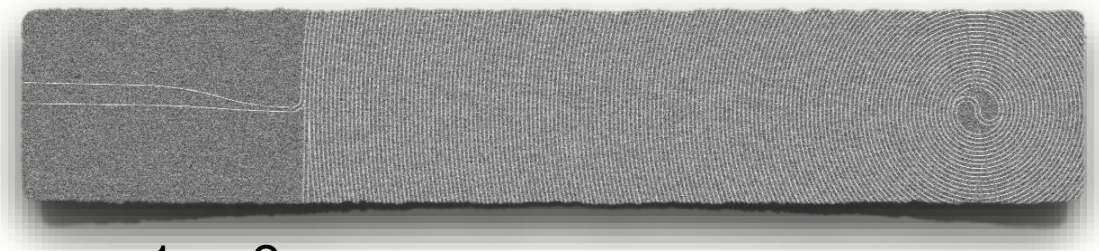

- Large area ~1mm2
- Requires relatively large currents
- Testing ongoing

Microfluidic source

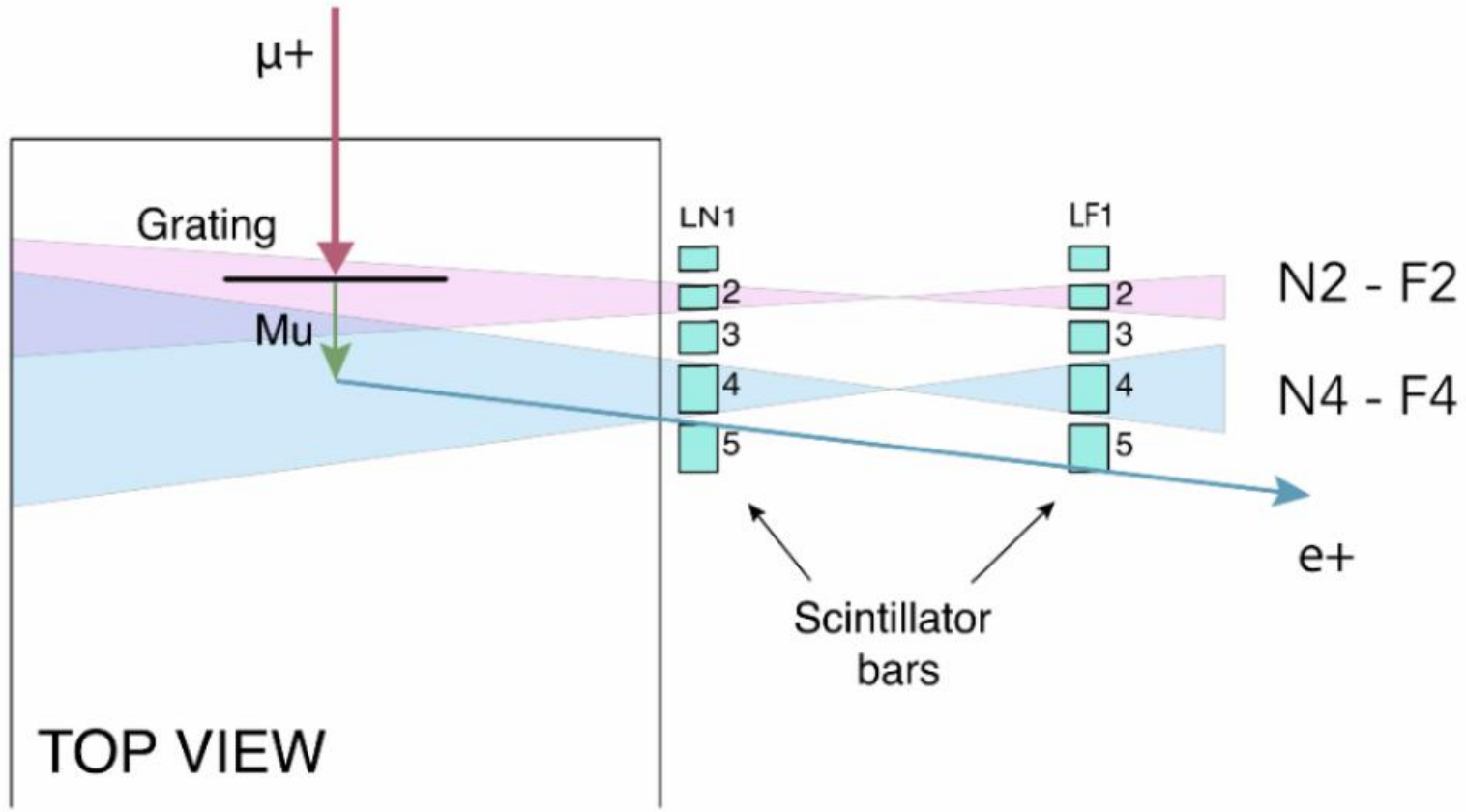

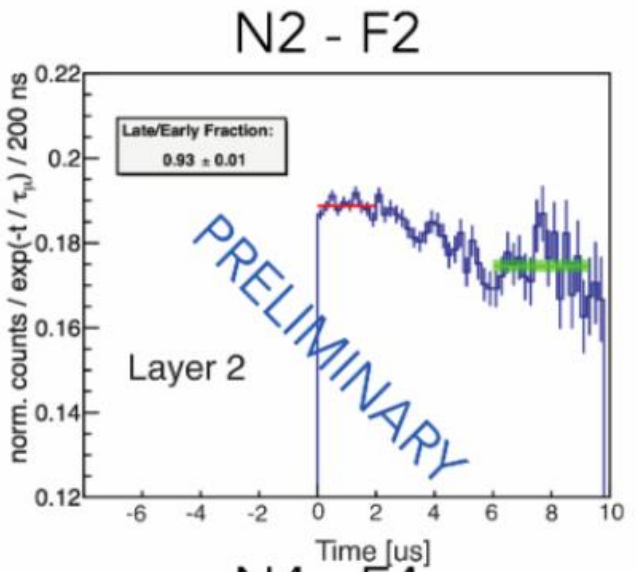

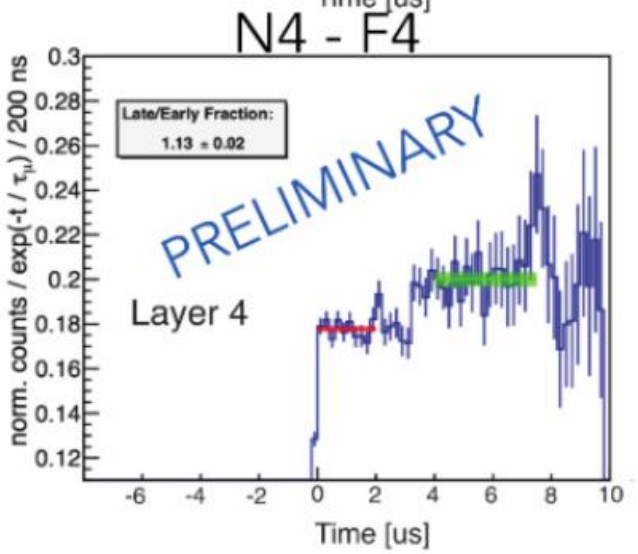

Parasitic rotation of the ball bearing interferometer

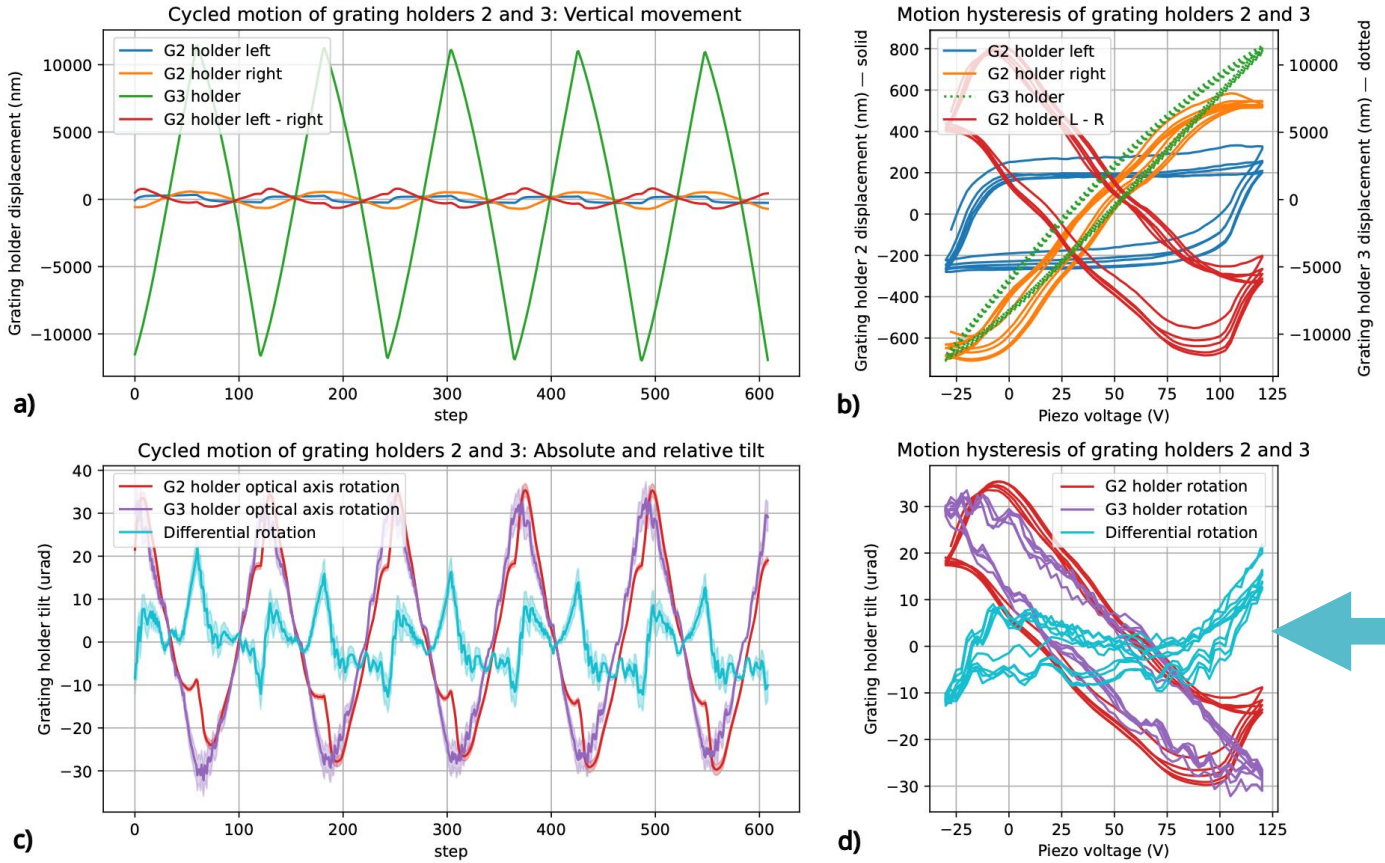

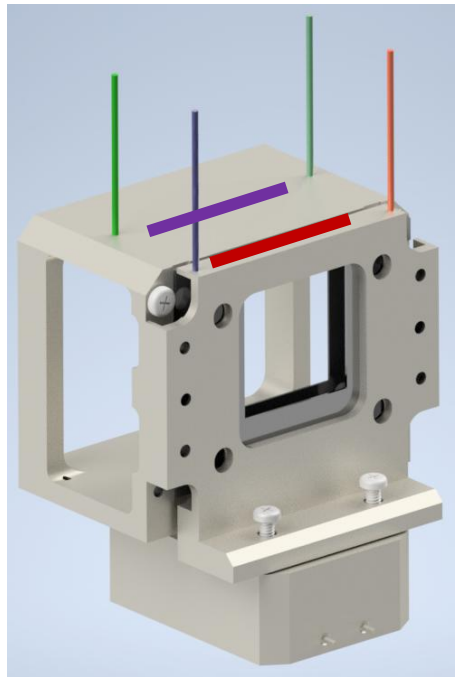

Differential rotation: 30μrad over 20μm

Require rotation $\theta_z < 160\mu$rad over 2μm

Simulation with GSM

- At z=0: $J(\boldsymbol{\rho}_a,\boldsymbol{\rho}_b;z)=\langle\psi^*(\boldsymbol{\rho}_b,z,t)\psi(\boldsymbol{\rho}_a,z,t)\rangle_t$

$$I^{(0)}(\boldsymbol{\rho};z)=J^{(0)}(\boldsymbol{\rho},\Delta\boldsymbol{\rho}=0;z)=\frac{w_{x0}}{w_x(z)}\frac{w_{y0}}{w_y(z)}e^{-\pi[x^2/w_x(z)^2+y^2/w_y(z)^2]}$$

With λ wavelength, w_0 beamwidth, l_0 transverse coherence length, r_0 radius of curvature of wave front

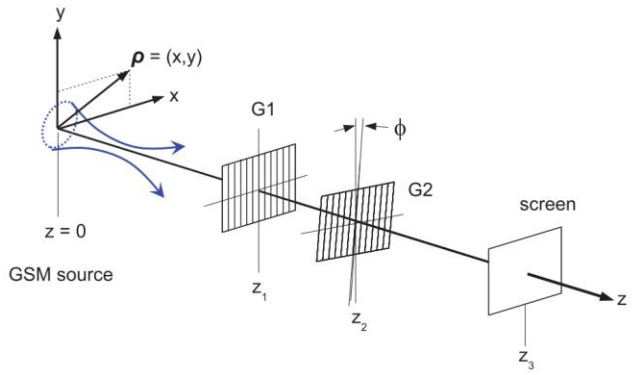

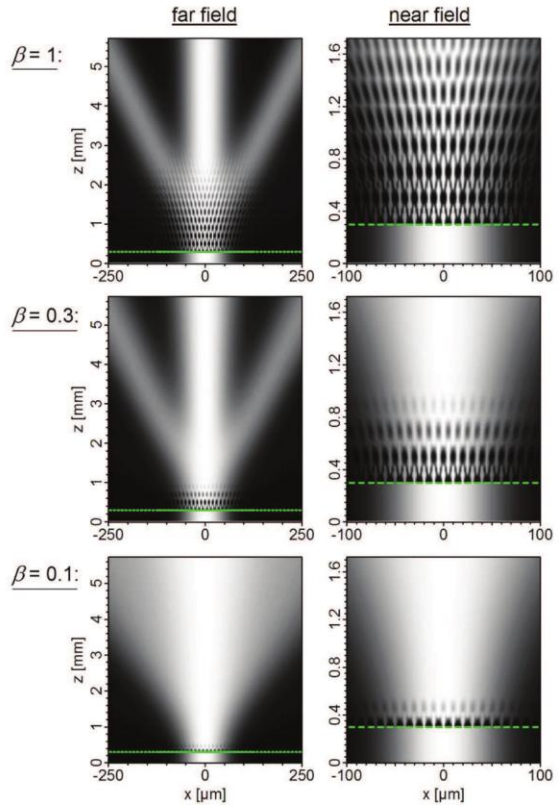

- After first grating: $t(\boldsymbol{\rho})=t(x)=\sum_{m=-\infty}^{\infty}a_m e^{-i2\pi mx/d_1}$

$$I^{(1)}(\boldsymbol{\rho};z_2)=J^{(1)}(\boldsymbol{\rho},\Delta\boldsymbol{\rho}=\mathbf{0};z_2)=\frac{w_{x0}}{w_x(z_2)}\frac{w_{y0}}{w_y(z_2)}e^{-\pi y^2/w_y(z_2)^2}\sum_{m,m'=-\infty}^{\infty}a^*_{m'}a_m\times e^{-\pi(x-\bar{m}\lambda z_{12}/d_1)^2/w_x(z_2)^2}$$
$$\times e^{-(i2\pi\Delta m/d_1)(x-\bar{m}\lambda z_{12}/d_1)(1-z_{12}/r_x(z_2))}\times e^{-\pi(\Delta m\lambda z_{12}/\ell(z_2)d_1)^2}$$

- After second grating:

$$I_{\mathrm{mf}}(x,z)=I_0\sqrt{\frac{\pi}{\Delta_v}}\sum_{m,n}a_m a_n\sqrt{\frac{\pi}{A}}e^{\frac{2\pi i}{d}(m-n)\bar{x}_{mn}\frac{\pi^2}{A\Delta_v}}e^{-\frac{\pi^2(m-n)^2(\lambda z)^2}{Ad^2}}\sum_{s=-\infty}^{\infty}e^{-\frac{(\bar{x}_{mn}-sd)^2}{2\sigma_I^2}\frac{\pi^2}{A\Delta_v}}e^{-\frac{2\pi i}{d}(m-n)sd\frac{\pi^2}{A\Delta_v}}$$

https://doi.org/10.1103/PhysRevA.78.013601

Simulation of incoherent array of periodic sources

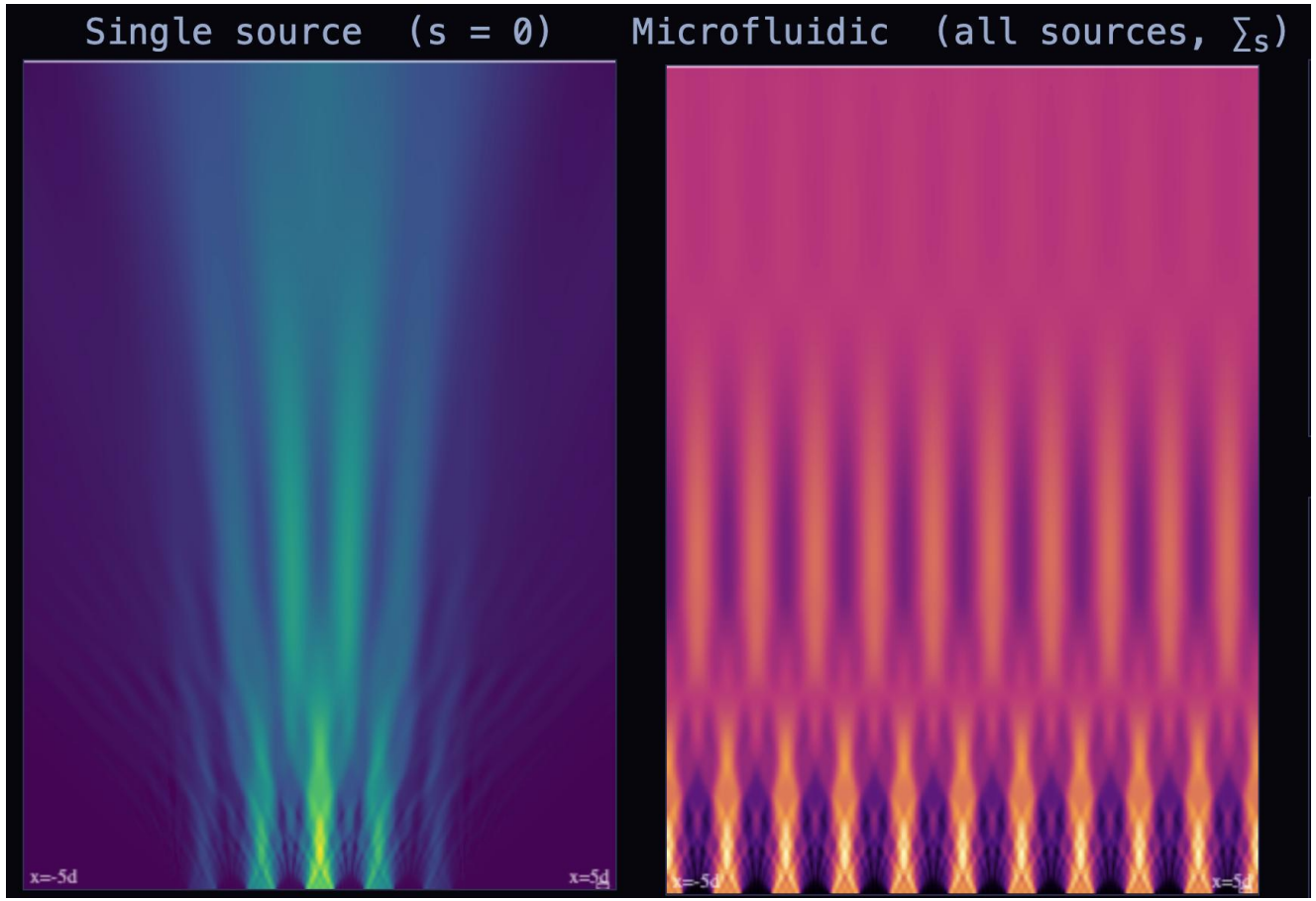

Phase I interferometer

-

First interferometry with Mu

-

Reduced alignment constraints allows the microfluidic Mu source to be the first optical grating

$$I_{\mathrm{mf}}(x,z) = I_0 \sqrt{\frac{\pi}{\Delta_v}} \sum_{m,n} a_m a_n \sqrt{\frac{\pi}{A}}\, e^{\frac{2\pi i}{d}(m-n)\bar{x}_{mn}\frac{\pi^2}{A\Delta_v}} e^{-\frac{\pi^2(m-n)^2(\lambda z)^2}{Ad^2}} \sum_{s=-\infty}^{\infty} e^{-\frac{(\bar{x}_{mn}-sd)^2}{2\sigma_I^2}\frac{\pi^2}{A\Delta_v}} e^{-\frac{2\pi i}{d}(m-n)sd\frac{\pi^2}{A\Delta_v}}$$

GSM simulations of the gravity interferometer

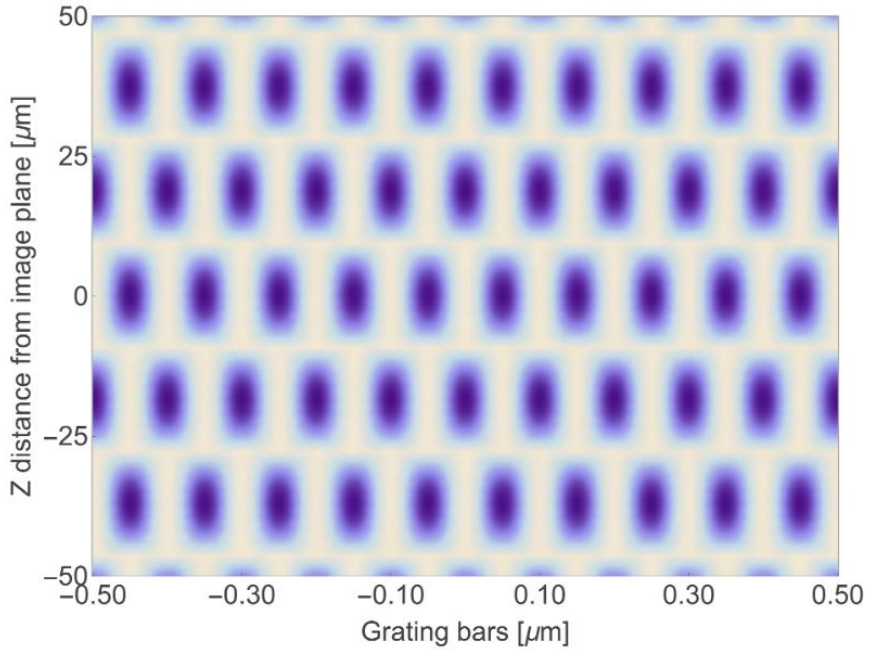

(a) Talbot contrast on the optical axis

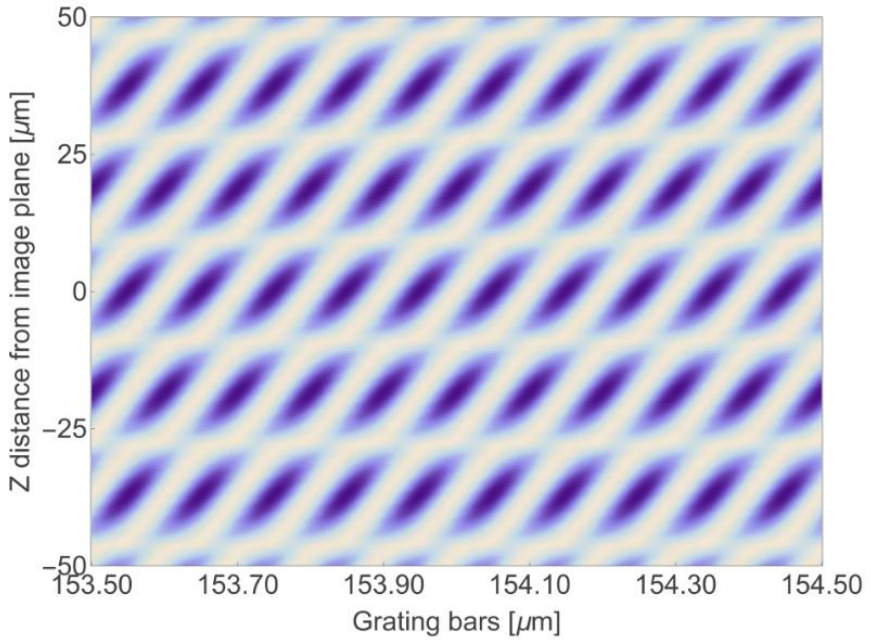

(b) At the position of the first Mach-Zehnder recombination from the Lau condition

Fig. 4.5 Comparison of the Talbot contrast on axis and shifted to the position of the Mach-Zehnder condition satisfied by the first diffraction. The contrast at both positions for this 4 grating setup is: ≈ 0.325.

LED test - Rotation

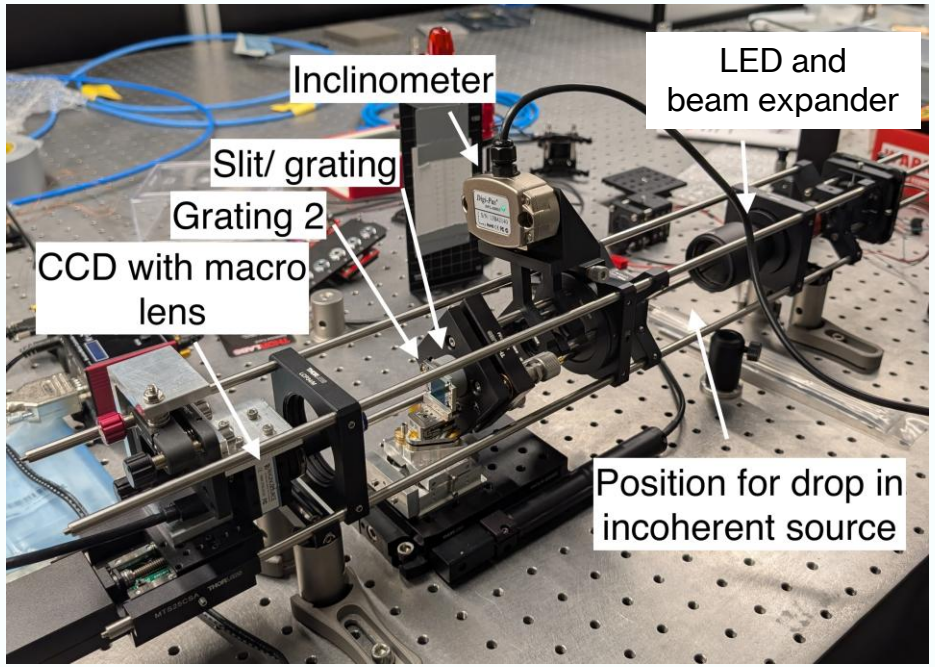

Laser shinning through a single slit and then a rotated grating

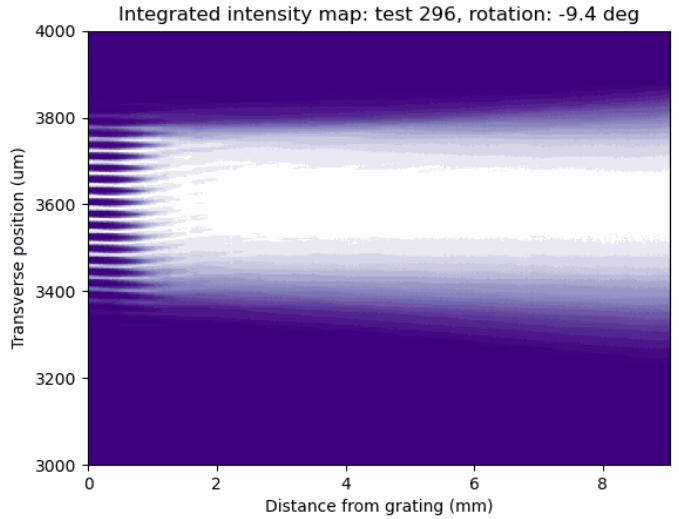

Experiment

Gaussian-Schell model with Mutual intensity function: :

$$I_{\mathrm{mf}}(x,z) = I_0 \sqrt{\frac{\pi}{\Delta_v}} \sum_{m,n} a_m a_n \sqrt{\frac{\pi}{A}}\, e^{\frac{2\pi i}{d}(m-n)\bar{x}_{mn}\frac{\pi^2}{A\Delta_v}} e^{-\frac{\pi^2(m-n)^2(\lambda z)^2}{Ad^2}} \sum_{s=-\infty}^{\infty} e^{-\frac{(\bar{x}_{mn}-sd)^2}{2\sigma_I^2}\frac{\pi^2}{A\Delta_v}} e^{-\frac{2\pi i}{d}(m-n)sd\frac{\pi^2}{A\Delta_v}}$$

https://doi.org/10.1103/PhysRevA.78.013601

Stability in the cryostat

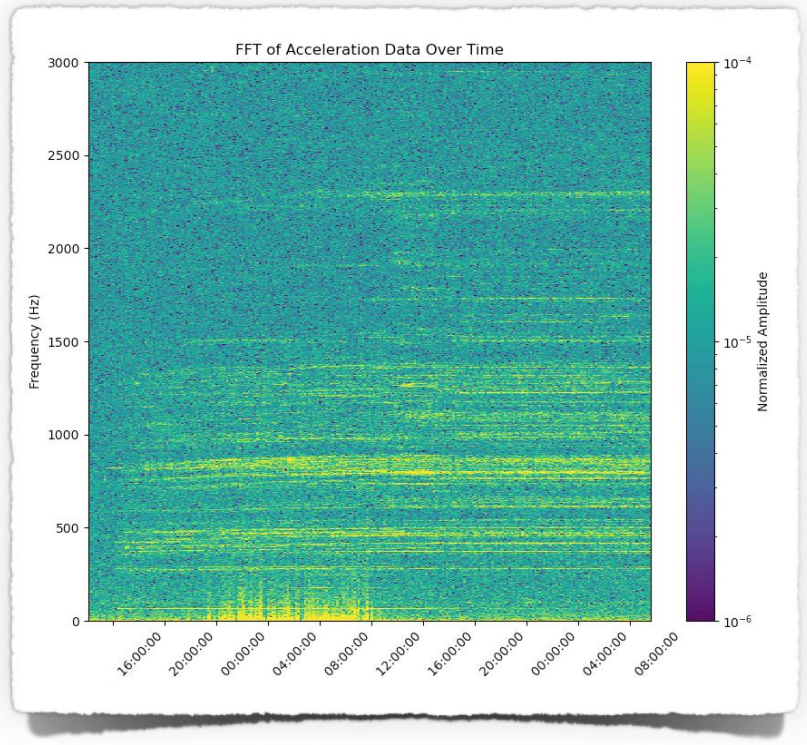

Vibration spectrum during cooldown

Turbomolecular pump

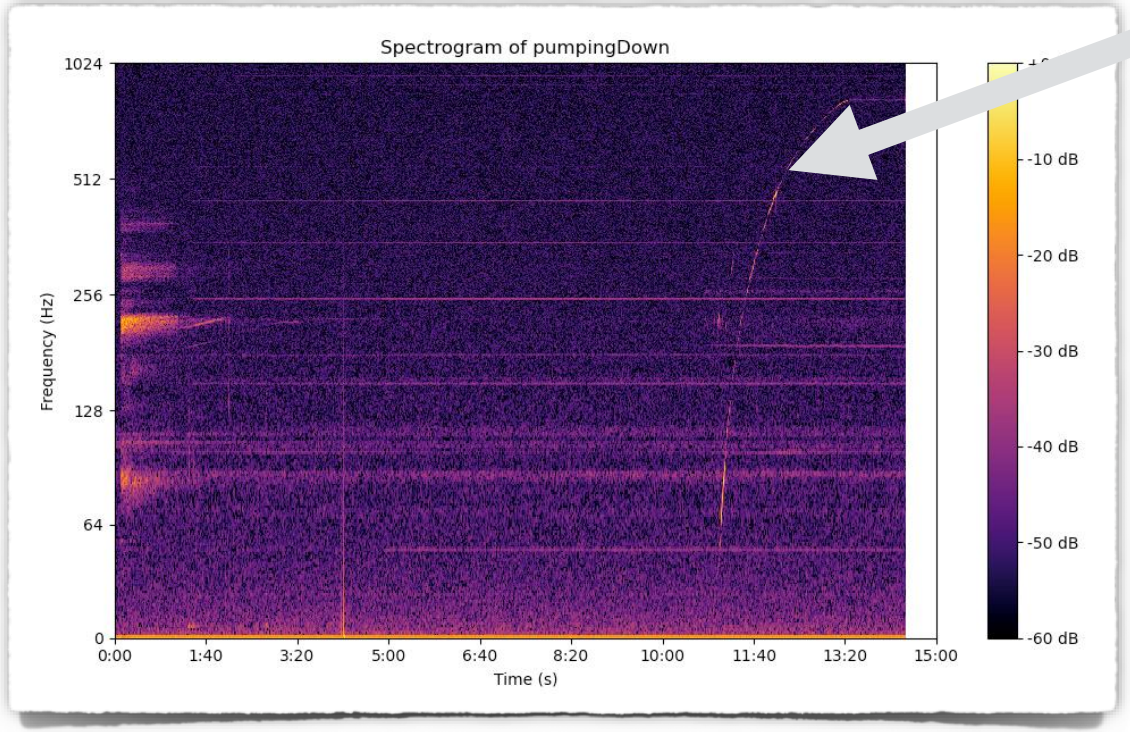

Vibration spectrum during evacuation

Made using cryogenic accelerometers